Atmos. Chem. Phys. Discuss., doi:10.5194/acp-2016-815, 2016
Manuscript under review for journal Atmos. Chem. Phys.
Published: 15 September 2016

Atmospheric Chemistry and Physics Discussions

Genesis of Diamond Dust and Thick Cloud Episodes observed above Dome C, Antarctica

Philippe Ricaud[1], Eric Bazile[1], Massimo del Guasta[2], Christian Lanconelli[3,4], Paolo Grigioni[5], Achraf Mahjoub[1]

[1]Météo-France/CNRM, CNRS UMR 3589, 42 avenue Gaspard Coriolis, 31057 Toulouse, France

[2]CNR, Via Madonna del Piano 10, 50019, Sesto Fiorentino, Italy

[3]Institute of Atmospheric Sciences and Climate (ISAC), Consiglio Nazionale delle Ricerche, via Gobetti 101, 40129 Bologna, Italy;

[4]Now at Joint Research Center, Institute for Environment and Sustainability (IES), Land Resource Management Unit (H05), via Fermi, 21027 Ispra (VA), Italy

[5]ENEA, Lungotevere Thaon di Revel, 76-00196 Roma, Italy

Version V7, 15 September 2016

To be submitted to: *Atmospheric Chemistry and Physics Discussions*

Atmos. Chem. Phys. Discuss., doi:10.5194/acp-2016-815, 2016
Manuscript under review for journal Atmos. Chem. Phys.
Published: 15 September 2016

Atmospheric Chemistry and Physics Discussions

Abstract

From 15 March to 8 April 2011 and from 4 to 5 March 2013, the atmosphere above Dome C (Concordia station, Antarctica, 75°06'S, 123°21'E, 3233 m amsl) has been probed by several instruments and model to study episodes of thick cloud and diamond dust (cloud constituted of suspended ice crystals). 1) A ground-based microwave radiometer (HAMSTRAD, H_2O Antarctica Microwave Stratospheric and Tropospheric Radiometers) installed at Dome C that provided vertical profiles of tropospheric temperature and absolute humidity to calculate Integrated Water Vapour (IWV). 2) Daily radiosoundings launched at 12:00 UTC at Dome C. 3) A tropospheric aerosol Lidar that provides aerosol depolarization ratio along the vertical at Dome C. 4) Down- and upward short- and longwave radiations as provided by the Baseline Surface Radiation Network (BSRN) facilities. 5) Space-borne aerosol depolarization ratio from the Cloud-Aerosol Lidar with Orthogonal Polarization (CALIOP) Lidar aboard the Cloud-Aerosol Lidar and Infrared Pathfinder Satellite Observation (CALIPSO) platform along orbits close to the Dome C station. The time evolution of the atmosphere has also been evaluated by considering the outputs from the meso-scale AROME and the global-scale ARPEGE meteorological models. Two distinct periods are highlighted by all the datasets: the warm and wet periods (24-26 March 2011 and 4 March 2013) and the cold and dry periods (5 April 2011 and 5 March 2013). Combining radiation and active measurements of aerosols with nebulosity calculations, a thick cloud is detected during the warm and wet periods with high depolarization ratios (greater than 30%) from the surface to 5-7 km altitude associated with precipitation of ice particles and the presence of a supercooled liquid water (depolarization of about 10%) cloud. During the cold and dry periods, high depolarization ratios (greater than 30%) to a maximum altitude of 100-500 m are measured suggesting that the cloud is constituted of ice crystals with no trace of precipitation. These ice crystals in suspension in the air are named diamond dust. Considering

Atmos. Chem. Phys. Discuss., doi:10.5194/acp-2016-815, 2016
Manuscript under review for journal Atmos. Chem. Phys.
Published: 15 September 2016

Atmospheric Chemistry and Physics Discussions

5-day back trajectories from Dome C and global distributions of IWV over the Antarctic show that the thick-cloud episode is attributed to air masses with an oceanic origin whilst the diamond dust episode is attributed to air masses with continental origins. This is consistent with ARPEGE temperature and water vapour tendency favouring predominantly advection processes including microphysical processes for water vapour.

Atmos. Chem. Phys. Discuss., doi:10.5194/acp-2016-815, 2016
Manuscript under review for journal Atmos. Chem. Phys.
Published: 15 September 2016

Atmospheric Chemistry and Physics Discussions

1. Introduction

The impact of global warming has become obvious in high latitude regions, particularly in the Arctic region, where melting ice and softening tundra are causing profound changes. The environmental response of the Arctic is characteristically different from that of the Antarctic because of differences in planetary geography and energy circulation. Over the past 50 years, the west coast of the Antarctic Peninsula has been one of the most rapidly warming parts of the planet. This warming is not only restricted to the land but can also be noted in the Southern Ocean. For example, the warming of the Antarctic winter troposphere is more important than anywhere on Earth with a rate of 0.5 to 0.7°C per decade measured over the last thirty years (Turner et al., 2006). In Antarctica, the polar vortex is more intense, is colder and lasts longer than in Arctic. The role of the Antarctic ice is important because it is one of the key parameters in the regulation of air temperature near the surface. During the austral winter, in the absence of solar radiation, the surface cools via infrared radiation emitted towards a very cold and very dry atmosphere. In the austral summer, the absorption of solar radiation at shorter wavelength produces a diurnal cycle and warms the surface while heating is limited by a high albedo (Pirazzini, 2004; Hudson et al., 2006).

Changes in the abundance of water vapour (H_2O) influence directly (and indirectly via clouds) the Earth's radiation budget and therefore affect climate change (Brasseur et al., 1999) because H_2O is the main greenhouse gas that emits and absorbs in the infrared domain. With an average altitude of 2500 m above sea level, the Antarctic Plateau is one of the coldest and driest places of the planet, for instance with temperature less than -80 °C and integrated water vapor amount less than 0.5 mm in winter at the Dome C station (e.g., Tomasi et al., 2012). For these reasons, numerous studies focused on climate change (e.g., Hines et al., 2004), processes in the atmospheric boundary layer (e.g., Argentini et al, 2005), reactive species

Atmos. Chem. Phys. Discuss., doi:10.5194/acp-2016-815, 2016
Manuscript under review for journal Atmos. Chem. Phys.
Published: 15 September 2016

74 interacting with the snow (e.g., Davis et al., 2001) and astronomical site quality (e.g.,
75 Tremblin et al, 2011).

76 Clouds also play an important role in the radiation budget of the Earth. Since they have
77 large spatial, seasonal and diurnal variability and they are poorly represented in climate
78 models, large differences are obtained by climate models when assessing the strength and the
79 direction of the cloud feedback on the Earth radiation balance (Dufresne and Bony, 2008).
80 The interconnections between the Antarctic, the middle latitudes and the tropics show that
81 Antarctic clouds are an important part of the global climate system (Lubin et al., 1998). Based
82 on observations from CloudSat and Cloud-Aerosol Lidar and Infrared Pathfinder Satellite
83 Observation (CALIPSO) satellites over the period 2006-2010 (Adhikari et al., 2012), it is
84 found that the Antarctic Plateau has the lowest cloud occurrence of the Antarctic continent
85 (<30%). The continental region of the Antarctic Plateau experiences cloud occurrence of
86 about 30% at low levels (less than 3 km) and less than 10% above 5 km whilst the western
87 continental region records cloud occurrence of about 50% at low levels and of about 30% up
88 to 8 km above the surface. Furthermore, whatever the season considered, it is shown that
89 multilayer clouds occur over Antarctica.

90 The Dome C station (Concordia) in Antarctica (75°06'S, 123°21'E, 3233 m above mean
91 sea level) is operated jointly by the French Polar Institute Paul-Emile Victor (IPEV) and the
92 Italian Institute Programma Nazionale Ricerche in Antartide (PNRA). The site is located on
93 the Antarctic plateau with 24 hours a day in summer and 24 hours of night in winter, a
94 climatological temperature between -40 °C and -20 °C in summer and -80° C and -60 °C in
95 winter (Tomasi et al., 2006). Situated on top of a dome, there is no katabatic wind as in the
96 case of the costal station of Dumont d'Urville (66°S, 140°E, 0 m above sea level) since the
97 average wind rarely exceeds 5 m s^{-1} throughout the year. When the temperature drops, water
98 may precipitate and light ice crystals may be suspended in the air producing a phenomenon

99 referred to as diamond dust. At the Dome C station, numerous studies already focused on the
100 diurnal and seasonal variations of the atmospheric boundary layer (e.g., Ricaud et al., 2012).
101 The main motivation of the present analysis is to investigate the presence of two different
102 clouds (thick cloud and diamond dust) that appeared above the Dome C station by combining
103 measurements from several instruments installed at the station, together with space-borne
104 measurements and model outputs. We intend to study the nature of the clouds and the
105 meteorological processes that favored their formation by using parameters such as
106 tropospheric temperature and absolute humidity, integrated water vapour, nebulosity, long-
107 and shortwave up- and downward radiations, together with the vertical distribution of aerosol
108 depolarization ratios.
109 We concentrate our efforts investigating two episodes: from 15 March to 8 April 2011 and
110 from 4 to 5 March 2013. Several instruments have been used. 1) A ground-based microwave
111 radiometer (HAMSTRAD, H_2O Antarctica Microwave Stratospheric and Tropospheric
112 Radiometers) installed at Dome C that provided vertical profiles of tropospheric temperature
113 and absolute humidity to calculate Integrated Water Vapour (IWV) with a 7-min integration
114 time. 2) Daily radiosoundings launched at 12:00 UTC at Dome C. 3) A tropospheric aerosol
115 Lidar that provides aerosol depolarization ratio along the vertical at Dome C. 4) Down- and
116 upward short- and longwave radiations as obtained from secondary standard pyranometers
117 and pyrgeometer installed at Dome C and belonging to the Baseline Surface Radiation
118 Network (BSRN). 5) Space-borne aerosol depolarization ratio from the Cloud-Aerosol Lidar
119 with Orthogonal Polarization (CALIOP) Lidar aboard the CALIPSO platform along orbits
120 close to the Dome C station. The time evolution of the atmosphere over the 1-month period in
121 2011 has also been evaluated by considering the outputs from the meso-scale model AROME
122 in 3 configurations. 1) “Operational”, operating mode with a snow albedo of 0.80. 2)
123 “Operational with ice tuning”, as in “Operational” but with a setting of snow albedo that can

Atmos. Chem. Phys. Discuss., doi:10.5194/acp-2016-815, 2016
Manuscript under review for journal Atmos. Chem. Phys.
Published: 15 September 2016

124 reach up to 0.85. And finally 3) “ARPEGE micro-physics”, as in “Operational with ice
125 tuning” but includes the physics of ARPEGE and a state-of-the-art scheme to represent the
126 snow pattern taking into account the roughness length. And finally, we will use the global-
127 scale ARPEGE meteorological analyses in 2013 selected over the Dome C station.

128 The manuscript is structured as follow. Section 2 presents all the data sets used in our
129 study. Section 3 investigates the episode 1, namely the thick cloud and the diamond dust
130 episodes during the 1-month period in 2011 considering the temporal evolution of the
131 different parameters above and in the surroundings of the Dome C station. Section 4 deals
132 with the episode 2 in 2013. The genesis of the formation of the thick cloud and the diamond
133 dust episodes is discussed in Section 5. Finally, Section 6 concludes the study.

134

135 ## 2. Datasets

136 ### 2.1. The HAMSTRAD Radiometer

137 The HAMSTRAD (H_2O Antarctica Microwave Stratospheric and Tropospheric
138 Radiometers) instrument is a state-of-the-art microwave radiometer to probe the troposphere
139 in very cold and very dry environments in order to retrieve temperature and absolute humidity
140 vertical profiles, and IWV. Temperature profiles are obtained from the 51–59 GHz spectral
141 range, centered on the oxygen line. Absolute humidity profiles are retrieved from the 169–197
142 GHz spectral range, centred on the water vapour line. IWV is calculated from the water
143 vapour profile integrated along the vertical. Integration time is 7 min. The radiometer is
144 presented in Ricaud et al. (2010).

145 The instrument was sent to Dome C in January 2009. It has been running automatically
146 since January 2010. Science and validation studies using HAMSTRAD data are detailed in
147 Ricaud et al., 2012; 2013; 2014a-c; and 2015. All the HAMSTRAD data measured since 2009
148 are freely available at the following address:

Atmos. Chem. Phys. Discuss., doi:10.5194/acp-2016-815, 2016
Manuscript under review for journal Atmos. Chem. Phys.
Published: 15 September 2016

http://www.cnrm.meteo.fr/spip.php?article961&lang=en. The radiometer sensitivity is very high in the planetary boundary layer, high in the free troposphere and very weak in the upper troposphere-lower stratosphere (Ricaud et al., 2015). The H_2O and temperature vertical resolutions are ~20-50 m, ~100 m and ~500 m in the planetary boundary layer, in the free troposphere and in the upper troposphere-lower stratosphere, respectively. Against radiosondes, there is a 1-5 K cold bias below 4 km, and a 5-10 K warm bias above. There is a wet bias of 0.1-0.3 g m^{-3} below about 2 km and a dry bias of ~0.1 g m^{-3} above. Integrated water vapour is of a high quality, 1-2% wetter than radiosondes.

2.2. Radiosondes

The programme of radiosoundings developed at Dome C is presented in Ricaud et al. (2014a). Temperature and humidity biases against HAMSTRAD are shown in the previous section. In the present study, the vertical profiles of temperature and humidity were taken from RS92 radiosondes using the standard Vaisala evaluation routines without any correction of sensor heating or time lag effect. We recall that the corrections performed on the radiosonde data measured in 2009 according to Miloshevish et al. (2006) shown a weak impact (with a maximum of +4% on IWV) on the vertical profiles (Ricaud et al., 2013). Furthermore, considering the updated tools developed in Miloshevich et al. (2009), Tomasi et al. (2011 and 2012) found that, between 630 and 470 hPa, the correction factor for humidity estimated by the radiosonde varied within 1.10-1.15 for daytime and within 0.98-1.00 for nighttime. It is important to note that the 630-470 hPa layer is located between the ground and an altitude of ~2 km which maximizes the calculation of IWV. A 1.2 K cold bias is also observed in the RS92 from the surface up to an altitude of ~4 km (Tomasi et al., 2011 and 2012).

Atmos. Chem. Phys. Discuss., doi:10.5194/acp-2016-815, 2016
Manuscript under review for journal Atmos. Chem. Phys.
Published: 15 September 2016

174 **2.3. The Aerosol Lidar**

175 The aerosol lidar is a backscatter and depolarization system in operation at Dome C in
176 relation with different scientific projects (http://lidarmax.altervista.org/lidar/ Antarctic
177 LIDAR.php). Vertical profiles of aerosol and cloud structures are continuously measured
178 together with the characterization of the physical phase of particles. Automated daily images
179 are produced and sent to Italy to monitor the state of the atmosphere above Dome C and to
180 check the instrument operations.

181 The Lidar system uses a Laser Quantel (Brio) at Dome C and operates at 532 nm to get
182 backscattering and depolarization ratio from 30 to 7000 m above ground with a 7.5-m vertical
183 resolution. The line of sight is zenith looking through a window enabling measurements in
184 all-weather conditions. The telescope has a 10-cm diameter, with 30-cm refractive optics and
185 0.15-nm interference filter. It has already been used in several scientific studies, e.g. the ra-
186 diative properties of H_2O and clouds in the far infrared over Antarctica (Palchetti et al., 2015).

187

188 **2.4. CALIOP onboard CALIPSO**

189 The CALIPSO satellite has been launched to study the role clouds and aerosols play in the
190 Earth system that includes air quality, weather and climate. CALIPSO was launched on 28
191 April 2006 with the cloud profiling radar system on the CloudSat satellite. The CALIPSO
192 satellite comprises three instruments, the CALIOP Lidar, the Imaging Infrared Radiometer
193 (IIR), and the Wide Field Camera (WFC) (Winker et al., 2009).

194 CALIOP is a two-wavelength (532 nm and 1064 nm) polarization-sensitive lidar that
195 provides high-resolution vertical profiles of aerosols and clouds
196 (https://calipso.cnes.fr/en/CALIPSO/lidar.htm). CALIOP uses three receiver channels: one
197 measures the 1064 nm backscatter intensity and two channels measure orthogonally polarized
198 components of the 532 nm backscattered signal. The receiver telescope is 1 metre in diameter.

Atmos. Chem. Phys. Discuss., doi:10.5194/acp-2016-815, 2016
Manuscript under review for journal Atmos. Chem. Phys.
Published: 15 September 2016

199 The full-angle field of view of the telescope is 130 µrad resulting in a footprint at the Earth's
200 surface of about 90 metres. Algorithms have been developed to retrieve aerosols and cloud
201 layers together with optical and microphysical properties (Young and Vaughan, 2009).
202 Depolarization ratio estimated with version V3.01 is presented in our study.
203
204 **2.5. The BSRN Network**
205 The objective of the World Climate Research Programme (WCRP) Baseline Surface
206 Radiation Network (BSRN) is to provide, using a high sampling rate, observations of the best
207 possible quality, for short- and longwave surface radiation fluxes. These readings are taken
208 from a small number of selected stations, including Dome C, in contrasting climatic zones,
209 together with collocated surface and upper air meteorological data and other supporting
210 observations. The incoming longwave and shortwave radiation components of the surface
211 radiative balance were taken from the Dome C BSRN station, and measured with two Kipp &
212 Zonen CM22 secondary standard pyranometers and two Kipp & Zonen CG4 Pyrgeometers,
213 all operated according to BSRN guidelines (Lanconelli et al., 2011).
214
215 **2.6. The AROME Model**
216 AROME (Seity et al., 2011) is a small-scale numerical prediction model, operational at
217 Meteo-France since December 2008. It was designed to improve short-range forecasts of
218 severe events such as intense Mediterranean precipitations (Cévenole events), severe storms,
219 fog, urban heat during heat waves. The physical parameterizations of the model come mostly
220 from the MESO-NH model whereas the dynamic core is the ALADIN model. The size of the
221 mesh is 2.5 km against 10 km for ARPEGE over France in 2014. The model is initialized
222 from a 3D-var data assimilation system using radar reflectivity and Doppler wind. Five daily
223 forecasts are made with AROME, thus helping to better predict meteorological events of the

Atmos. Chem. Phys. Discuss., doi:10.5194/acp-2016-815, 2016
Manuscript under review for journal Atmos. Chem. Phys.
Published: 15 September 2016

day and of the morrow (30 h forecast range). AROME was used within the project GEWEX Atmospheric Boundary Layer Study 4 (GABLS4) whose one of the motivations was the study of the meteorological evolution over the Dome C station (Bosveld et al., 2014).

For the study, three experiments at 2.5 km were used. Two based on the AROME configurations: 1) "Operational", operating mode with the default snow scheme (Douville et al., 1995) (labeled as 79HA). 2) “Operational with ice tuning”, as in “Operational” but with a setting of a minimum snow albedo of 0.8 (labeled as 79YG). In the third one “ARPEGE microphysics”, the AROME physics was replaced by the ARPEGE one used in the global model with the state-of-the-art scheme to represent the permanent snow with a minimum snow albedo of 0.8 valid over Dome C and a more accurate roughness length (labeled as 79Z6).

2.7. The ARPEGE Model

The ARPEGE model is the global model used for the numerical weather prediction (NWP) at Météo-France. In the present study, the operational configuration has been used with a stretched grid at high resolution over France (10 km) and a coarser grid over Australia of 60 km. At the South Pole, the horizontal resolution is about 50 km and the vertical grid has 70 levels with a first level at around 16 m above the ground. The assimilation tool is based on an incremental 4-dimensional variational (4D-Var) method. The physical package used in the ARPEGE model is at the state-of-the-art, with a Turbulent Kinetic Energy scheme associated with a mass flux scheme for the boundary layer (Bazile et al., 2011). The clouds and the micro-physics use 4 prognostic variables such as cloud water, cloud ice, rain and snow (Lopez, 2002; Bouteloup et al., 2005). The radiative transfer in the atmosphere is computed with the Rapid Radiative Transfer Model (RRTM) scheme (Mlawer et al., 1997) for the longwave and the shortwave with the Fouquart-Morcrette scheme (Fouquart and Bonnel, 1980; Morcrette et al., 2001).

Atmos. Chem. Phys. Discuss., doi:10.5194/acp-2016-815, 2016
Manuscript under review for journal Atmos. Chem. Phys.
Published: 15 September 2016

Atmospheric Chemistry and Physics Discussions

249

250 3. Episode 1 on 15 March-8 April 2011

251 3.1. Temperature

252 Figure 1 shows the time evolution of temperature from 15 March to 8 April 2011 in the
253 planetary boundary layer at 4, 50 and 100 m above the ground as measured by HAMSTRAD,
254 the radiosondes and as calculated by AROME according to the 3 configurations detailed in
255 the previous section, namely a) operational, b) operational with ice tuning and c) considering
256 ARPEGE micro-physics. Unless explicitly specified, from now, all the heights refer to height
257 above the ground. The time evolution of temperature profiles as measured by HAMSTRAD
258 from 0 to 5 km is shown Fig. 2.

259 In the planetary boundary layer (Fig. 1), temperatures from HAMSTRAD and the
260 radiosondes are rather stable from 15 to 24 March 2011 (210-220 K at 4 m), rapidly increase
261 to ~240 K on 25 March and start decreasing on 26 March to 31 March (~210 K). After a
262 slight increase on 4 April (~220 K), a minimum in temperature is reached on 5 April (210 K
263 at 50 and 100 m) with stable temperature at 4 m while increasing at 50 and 100 m reinforcing
264 the inversion. The sharp increase in temperature measured at 4 m (~30 K) on 25 March is
265 much less intense above, at 50 and 100 m (~5 K), but the sharp decrease in temperature on 5
266 April is much more intense at 50 and 100 m (~20 K) than at 4 m (~10 K maximum). At 50
267 and 100 m, measurements from HAMSTRAD and radiosondes are very consistent with the
268 outputs from AROME whatever the configuration considered. But there are some differences
269 at 4 m. The biggest differences are detected during the period 20-25 March, prior to the warm
270 period 25-26 March, during which AROME outputs are systematically greater than the
271 measurements by 10-15 K whatever the configuration considered. During the other periods,
272 although the operational AROME outputs (79HA) are warmer than the outputs from the two
273 other configurations by 2-3 K on average at 06:00 UTC (14:00 LT), the outputs from

Atmos. Chem. Phys. Discuss., doi:10.5194/acp-2016-815, 2016
Manuscript under review for journal Atmos. Chem. Phys.
Published: 15 September 2016

AROME version ARPEGE micro-physics (79Z6) around 16:00 UTC (local midnight) is warmer than the two other configurations on few periods (16-25 March and 2, 4, 7 and 9 April). At 12:00 UTC (20:00 LT), the outputs from 79Z6 are the closest to the radiosonde and the HAMSTRAD measurements. We note a diurnal cycle in temperature of ±3 K observed in the AROME outputs from the operational configuration that is not present in the HAMSTRAD data set. Above, at 50 and 100 m, all the data sets considered are very consistent to each other within ±2 K.

From 0 to 5 km (Fig. 2), the two episodes of abrupt changes in temperature are clearly detected on 25 March and on 5 April 2011, with substantial increase and decrease in temperature, respectively. Along the vertical, these two episodes cover a wide domain from the ground to more than 3 km. The warm episode lasts 3-4 days although the cold episode is of a short duration, namely 1 day.

3.2. Integrated Water Vapour

If we now consider the evolution of IWV over the same period (Fig. 3), we note a slight positive change from 15 to 22 March 2011 (from 0.3 to 0.6 kg m^{-2}), followed by an abrupt increase on 25 March of 1.0 kg m^{-2} in less than 24 hours. After a 2-day plateau at 1.4 kg m^{-2} in HAMSTRAD and radiosonde data, IWV decreases slowly until the end of the period. Neverthless, on 5 April, the atmosphere is the driest of the period reaching 0.1 kg m^{-2} within few hours. All the data sets (HAMSTRAD, radiosonde and AROME) behave consistently during this period. HAMSTRAD and the radiosonde data do not exhibit any bias, whilst AROME outputs tend to show a much wetter atmosphere compared to HAMSTRAD and the radiosondes of about 0.2 kg m^{-2}, except during the warm and wet period (25-26 March) when the bias is even greater reaching 0.4-0.5 kg m^{-2}.

Atmos. Chem. Phys. Discuss., doi:10.5194/acp-2016-815, 2016
Manuscript under review for journal Atmos. Chem. Phys.
Published: 15 September 2016

3.3. Absolute Humidity

Figure 4 shows the time evolution of absolute humidity vertical profiles from 15 March to 8 April 2011 in the planetary boundary layer (4, 50 and 100 m) as measured by HAMSTRAD, the radiosondes and as calculated by AROME according to the 3 configurations. The time evolution of absolute humidity as measured by HAMSTRAD from the ground to 5 km is shown Fig. 5.

Consistently with the time evolution of IWV, the evolution of absolute humidity in the planetary boundary layer (Fig. 4) and in the free troposphere (Fig. 5) shows an abrupt increase on 25 March and a net decrease on 5 April, but with lots of differences within all the datasets and the altitude layers considered. Prior to the warm and wet episode of 25-26 March, HAMSTRAD measurements from 4 to 100 m (Fig. 5) are systematically much wetter than both the radiosondes and the AROME outputs by 0.1-0.2 g m^{-3} and 0.4-0.5 g m^{-3}, respectively. It is a very well documented bias already presented in several works (e.g. Ricaud et al., 2014a and 2015) that HAMSTRAD measures a wetter atmosphere below 2 km and drier above, than any other data sets (radiosonde, in situ, space-borne, and meteorological analyses). After the warm and wet period, the bias reduces to 0.1 g m^{-3} between HAMSTRAD and the radiosondes. We note some differences in the H_2O time evolution within the AROME outputs according to the 3 configurations. The operational outputs (79HA) are usually much wetter than the two other configurations, particularly around local noon and in the lowermost layer at 4 m. The biases within the outputs of the 3 configurations decrease with height.

Along the vertical (Fig. 5), the time evolution of the H_2O field obviously shows the two episodes of abrupt changes detected on 25 March and on 5 April 2011, with a net increase and a net decrease in H_2O, respectively. These two episodes cover a wide domain from the ground up to 2.5-3 km. Consistently with the conclusions drawn with temperature evolution in the

Atmos. Chem. Phys. Discuss., doi:10.5194/acp-2016-815, 2016
Manuscript under review for journal Atmos. Chem. Phys.
Published: 15 September 2016

Atmospheric Chemistry and Physics Discussions

section 3.1, the wet and warm episode (see Fig. 2) lasts 2-3 days although the cold and dry episode is of a short duration, namely less than 1 day.

3.4. Radiation

The time evolution of the downward and upward short- and longwave radiations as measured by the BSRN international network is displayed in Figure 6, together with the net irradiance (difference between the downward and the upward fluxes) from 15 March to 8 April 2011. The diurnal cycle of solar irradiance fluxes is clearly evidenced with the obvious maximum at local noon ranging between 350 W m^{-2} (at the beginning of the period) and 150 W m^{-2} (at the end of the period). Albedo over the whole period is found to range between 0.8 and 0.95 with daily minimum at local noon (not shown). The upward longwave radiation emitted by the surface is generally greater than the downward irradiance in clear sky conditions, while they became similar under overcast when thick cloudiness prevents radiative cooling. Consequently, alternating day and night periods in March and April, the net irradiance is negative except around local noon when it can be either positive or close to zero. But for the two periods considered so far, namely on 25-26 March (warm and wet) and on 5 April (cold and dry), the radiation budget is significantly different from the average situation.

On 25 March, the longwave radiations (both downward and upward) are much greater than the shortwave radiations (both downward and upward) even at local noon. The resulting effect is that the net irradiance is positive or close to zero over the whole period. This obviously indicates that a thick cloud is shielding the downward shortwave radiation (coming from the Sun) and increases the downward longwave radiation (coming from the cloud). Furthermore, there is a great probability a thick cloud is present over the Dome C station during the warm and wet period.

Atmos. Chem. Phys. Discuss., doi:10.5194/acp-2016-815, 2016
Manuscript under review for journal Atmos. Chem. Phys.
Published: 15 September 2016

On 5 April during the cold and dry period, the situation is radically different. There is not an abrupt increase of longwave downward radiation as it was the case during the warm and wet period, so we can rule out the presence of a thick cloud above the station. Nevertheless, the situation is atypical since, at local noon, the downward shortwave radiation is only slightly greater than the upward shortwave radiation, and the net irradiance does not exhibit an obvious diurnal cycle maximizing at local noon. Consequently, even if the presence of a thick cloud has been ruled out from the longwave radiation analysis, both the shortwave and the total irradiance analyses tend to suggest the presence of a cloud, probably thin and/or close to the surface, in order to 1) slightly affect the downward longwave irradiance, and 2) strongly affect the diurnal cycle of the net irradiance. The next section investigates the presence and the nature of the clouds during the two periods under consideration: a) the warm and wet period (25-26 March 2011) and b) the cold and dry period (5 April 2011).

3.5. Clouds

The time evolution of the nebulosity vs. height as calculated by AROME according to the 3 configurations over the period 25 March-8 April 2011 is displayed Figure 7. In two configurations (operational and operational with ice tuning), clouds (traced by values of nebulosity greater than 0.25) are calculated mainly over two single periods: 1) on 22 March from 1 to 5 km, and 2) on 25-29 March from the ground to 6 km. Considering the third configuration (ARPEGE microphysics), the period when clouds (traced by values of nebulosity greater than 0.25) are present is much longer than the two first configurations since it almost covers the entire time interval under consideration. There are indeed the two periods previously cited, namely on 22 March, and 25-29 March, but they extend both in time (22-24 March and 25-30 March, respectively) and altitude (surface to 7 km). Other periods show some moderate values of nebulosity (0.10-0.25) on 15-17, 20 March, and 2, 3, 4, 6-7 April.

Atmos. Chem. Phys. Discuss., doi:10.5194/acp-2016-815, 2016
Manuscript under review for journal Atmos. Chem. Phys.
Published: 15 September 2016

These calculated clouds can be close to the ground or high in the free troposphere (4-6 km). In the three configurations, high nebulosity values (greater than 0.8) are calculated close to the surface (0-200 m). The AROME model tends to produce a sort of cloud residual in the planetary boundary layer in the three configurations analyzed.

The warm and wet period (25-26 March 2011) highlighted in the previous sections is indeed characterized by high values of nebulosity (greater than 0.8) whatever the configurations of AROME considered, from the surface to 6-7 km. This is another indicator of the presence of a thick cloud over the Dome C station during that period. The cold and dry period (5 April 2011) is nevertheless not characterized by such a high value of nebulosity extending in the free troposphere but rather by some high nebulosity being confined below 100 m. But this is probably an artifact of all the runs performed by ARPEGE within the 3 configurations, producing a residual cloud in the lowermost planetary boundary layer.

In order to check whether clouds are present or not over the station during the two periods studied in detail, we consider now the time evolution of the aerosol depolarization as measured by the Lidar installed at Dome C on 24-26 March and on 4-6 April 2011 (Fig. 8). For the warm and wet period (Fig. 8 top), high depolarization ratios (greater than 30%), signature of ice particles, start increasing by the end of 24 March (22:00 UTC), reaching an altitude of 1.2-1.5 km, all over 25 March, and start decreasing on 26 March by 12:00 UTC. The vertical structures in the depolarization ratio fields are a signature of precipitation of ice particles (Mishchenko et al., 2000). On 26 March, at about 2 km altitude from 07:00 to 13:00 UTC, a layer of low depolarization ratio (less than 14%) appears, that is a signature of liquid water cloud. In general, over this period, the cloud is so opaque that the Lidar signal cannot penetrate the structure beyond ~1.2 km altitude.

We may have a better insight in the vertical structure of the cloud covering the Dome C station on that warm and wet period by considering the space-borne CALIOP Lidar nighttime

Atmos. Chem. Phys. Discuss., doi:10.5194/acp-2016-815, 2016
Manuscript under review for journal Atmos. Chem. Phys.
Published: 15 September 2016

measurements performed on 25 March 2011 in the vicinity of the station. Figure 9 top left shows the Spaceborne Lidar CALIOP measurements of depolarization ratio along one orbit in the vicinity of the Dome C station on 25 March 2011. We note that, at the location of the Dome C station (75°06'S, 123°21'E), the depolarization ratio is greater than 0.4 (ice particles) from the ground (3233 m above mean sea level, amsl) to about 10 km amsl, namely ~7 km above the ground. If we now combine the downward and upward Lidar information, we can state that on the warm and wet period (24-26 March 2011), a 7-km thick ice cloud passed over the Dome C station and precipitated ice particles whilst, by the end of the period, a low-altitude (~2 km) liquid water cloud was also present.

For the cold and dry period (centered on 5 April 2011), high depolarization ratios (greater than 30%) from the Lidar operating at Dome C (Fig. 8 bottom) start increasing by the middle of 4 April (12:00 UTC), reaching a maximum altitude of 100 m, increasing up to 200 m on 5 April at 09:00 UTC, to finish decreasing on 6 April by 12:00 UTC. The high depolarization ratio suggests that the cloud is constituted of ice crystals and, since there is no vertical layers (as during the warm and wet period), there is no trace of precipitation. Considering the CALIOP space-borne Lidar measurements of depolarization ratio (Fig. 9 top right) performed on 5 April 2011 in the vicinity of the Dome C station, they also suggest a much thinner cloud from the ground to about 4 km amsl, namely less than 1 km above the ground, with values ranging 0.1-0.2 (ice particles). Since there is no precipitation and no presence of standard thick clouds above the station, the thin cloud episode is traditionally attributed to a diamond dust episode, rather frequent at the Dome C station.

Diamond dust is usually made of ice crystals in suspension in the air located in the lowermost troposphere. At the South Pole station, when sorted by number, Lawson et al. (2006) attributed 45% of the ice crystals recorded to diamond dust (columns, thick plates and plates), 30% are rosette shaped (mixed-habit rosettes, plate-like polycrystals and rosette

Atmos. Chem. Phys. Discuss., doi:10.5194/acp-2016-815, 2016
Manuscript under review for journal Atmos. Chem. Phys.
Published: 15 September 2016

shapes with side planes) whilst 25% are irregular. In the Eastern Antarctic Plateau over all the seasons except summer, a strong surface-based temperature inversion persists in which vertical mixing causes the boundary-layer air to become supersaturated with respect to ice. Consequently, small ice crystals referred to as diamond dust form in this layer (Walden et al., 2003). Nevertheless, even in the absence of mixing, longwave cooling of the near-surface air can also lead to supersaturation with respect to ice and form ice crystals. Classification of ice-cloud particles is important to retrieve the shape of individual crystals and to estimate the radiative impact of the clouds (Bailey and Hallett, 2009; Lindqvist et al., 2012). It is beyond the scope of the present analysis to classify ice crystals measured over the Dome C station.

4. Episode 2 on 4-5 March 2013

The second episode is much shorter than the first one since it lasts only two days from 4 to 5 March 2013. It relies on the same datasets as presented in section 3 except that the analyses are from the meteorological operational model ARPEGE that routinely delivers since December 2011 every 6 hours (00:00, 06:00, 12:00, and 18:00 UTC) meteorological fields at the vicinity of the Dome C station.

4.1. Temperature

The temperature anomaly over the 2-day period is represented in the Figure 10 as measured by HAMSTRAD and as calculated by ARPEGE. From the surface to about 2 km altitude, they both show a warm period on 4 March followed by a cold period on 5 March, with a transition propagating in the HAMSTRAD data up to 4 km altitude, probably due to the vertical resolution of the microwave radiometer measurements. Above this altitude, a cold period is followed by a warm period in the two datasets. Although the HAMSTRAD data are noisier than the ARPEGE data, the maxima and minima are consistently observed and

447 calculated in the lowermost troposphere around 12:00-18:00 UTC on 4 March and around
448 18:00-22:00 UTC on 5 March, respectively.
449
450 **4.2. Water Vapour**
451 The water vapour anomaly over the 2-day period is represented in the Figure 11 as
452 measured by HAMSTRAD and as calculated by ARPEGE. From the surface to about 4-5 km
453 altitude, they both show a wet period on 4 March followed by a dry period on 5 March. As for
454 temperature, the HAMSTRAD H_2O data are noisier than the ARPEGE data, but the maxima
455 and minima are consistently observed and calculated in the lowermost troposphere around
456 12:00-18:00 UTC on 4 March and around 18:00-22:00 UTC on 5 March, respectively.
457
458 **4.3. Radiation**
459 The time evolution of the downward and upward short- and longwave radiations as
460 measured by the BSRN international network is displayed in Figure 12, together with the net
461 irradiance (difference between the downward and the upward fluxes) from 1 to 9 March 2013.
462 As already presented in section 3.4, the diurnal cycle of solar irradiance fluxes mainly shows
463 a clear-sky period over the Dome C station, except over the period from 4 March at 00:00
464 UTC to 6 March at 00:00 UTC. Indeed, on 4 March all day long, there is a net increase in the
465 longwave downward radiation from 80 to 120 W m^{-2} compared to the values from 1 to 3
466 March and from 7 to 9 March when we can expect the station is under clear sky conditions.
467 Furthermore, from 12:00 to 24:00 UTC, the net irradiance is about –20 W m^{-2} on 4 March,
468 whilst it is usually about –30 W m^{-2} in clear sky conditions. Consequently, there is a great
469 probability a thick cloud is present over the Dome C station on 4 March during 24 h.
470 On 5 March, between 12:00 and 24:00 UTC, the net irradiance is very low (about –50 W
471 m^{-2}) compared to values of about –30 W m^{-2} in clear sky conditions. There is a slight increase

Atmos. Chem. Phys. Discuss., doi:10.5194/acp-2016-815, 2016
Manuscript under review for journal Atmos. Chem. Phys.
Published: 15 September 2016

of the longwave downward (90 W m^{-2}) and upward (140 W m^{-2}) fluxes on 5 March compared to the fluxes in clear sky conditions (70 and 120 W m^{-2}, respectively), but much less than fluxes in cloudy conditions (150 and 160 W m^{-2}, respectively). Consequently, this period of 12 hours on 5 March cannot be attributed to neither clear sky nor thick cloud episodes.

4.4. Clouds

Now we consider the presence of clouds and/or ice/liquid particles over the 2-day period either from active and passive remote-sensing measurements or from ARPEGE analyses. The time evolution of ice water mixing ratio calculated by ARPEGE over Dome C is represented in the Figure 13 top together with the total precipitation flux over the 2-day period (Fig. 13 bottom). ARPEGE analyses obviously calculate ice cloud from the surface to an altitude of about 4 km on 4 March, with a top altitude decreasing down to the surface on 5 March at 12:00 UTC. Between 18:00 and 24:00 UTC on 5 March, there is also a trace of ice cloud from 0 to 1 km altitude. The main thick cloud calculated on 4 March is associated with ice precipitation from the altitude of ~3 km at 06:00 UTC down to ~2 km on 20:00 UTC (Fig. 13 bottom). There is no longer trace of local precipitation after 03:00 UTC on 5 March.

The depolarization ratio measured by the aerosol Lidar installed at Dome C from 4 to 5 March is shown on Figure 14. For the warm and wet period (4 March), high depolarization ratios (greater than 30%) are present all over 4 March, reaching an altitude of 1.5-2.0 km, and start decreasing on 5 March by 00:00 UTC. The vertical structures in the depolarization ratio fields are a signature of precipitation of ice particles. Between 13:00 and 14:00 UTC on 4 March and from 00:00 to 10:00 UTC on 5 March, depolarization ratios are much lower, reaching values of less than 10%. This is clearly the signature of the presence of supercooled liquid water. From 10:00 to 24:00 UTC on 5 March, depolarization ratios are very high (>40%), indicative of ice crystals, but confined from the surface to 100-200 m altitude. There

Atmos. Chem. Phys. Discuss., doi:10.5194/acp-2016-815, 2016
Manuscript under review for journal Atmos. Chem. Phys.
Published: 15 September 2016

is no vertical structures, it means there is no precipitation associated to the presence of the cloud. Furthermore, this ice crystals can be considered as in suspension in the air and labeled as “diamond dust”. This is confirmed by the BSRN radiation measurements (see section 4.3).

Over this 2-day period, only one CALIOP/CALIPSO orbit has been analyzed in the vicinity of the Dome C station (Fig. 9 bottom) on 4 March (08:15 UTC) during the thick-cloud episode. On that day, the depolarization ratio is ranging 0.1-0.3 from the ground (3233 m amsl) to about 8 km amsl, namely ~5 km above the ground. Note that there is no CALIPSO orbit in the vicinity of the Dome C station in coincidence with the diamond dust episode.

If we synthesize our findings relative to the episodes 1 and 2, we can state the following. The time evolution of temperature, absolute humidity, ice and aerosol fields obviously shows two episodes of abrupt changes. Firstly, a warm and wet period is associated with a thick cloud that develops from the surface to 5-8 km and is constituted of ice crystals that precipitate. Secondly, a cold and dry period is associated with a thin cloud that develops close to the surface (100-200 m) and is constituted of ice crystals in suspension in the air. This later episode is known as “diamond dust” episode.

5. Discussions

In this section, we investigate the processes that contributed to the presence of a thick-cloud and a diamond-dust episode above the Dome C station considering the origin of air masses, the integrated water vapour fields over Antarctica and the temperature and water vapour budgets calculated by ARPEGE.

5.1. Origin of Air Masses

The impact of the origin of air masses on the short-term variability of H_2O and temperature and the high correlation coefficient (greater than 0.90) between water vapour and temperature

Atmos. Chem. Phys. Discuss., doi:10.5194/acp-2016-815, 2016
Manuscript under review for journal Atmos. Chem. Phys.
Published: 15 September 2016

522 at Dome C over the entire year 2010 were presented in Ricaud et al. (2012 and 2014c) based
523 on 5-day back-trajectory calculations. We propose, in the present study, to use the same
524 methodology to interpret the time evolution of the atmosphere during the two above-
525 mentioned episodes. We have thus considered a 5-day back trajectory study based upon the
526 European Centre for Medium-Range Weather Forecasts (ECMWF) analyses starting from the
527 Dome C location at five different pressure levels from the planetary boundary layer (650 and
528 600 hPa), to the free troposphere (500, 400 and 300 hPa).

529 For episode 1, Figure 15 (top left) shows the 5-day back-trajectories at the 5 selected
530 pressure levels during the warm and wet period (see the section 3) on 25 March 2011 at 12:00
531 UTC corresponding to the time of maximum temperature and absolute humidity of an air
532 parcel issued from Dome C. In the lowermost layers (650 and 600 hPa), the air parcels are
533 mainly issued from the Antarctic continent. But higher up, at 500, 400 and 300 hPa, air
534 masses are coming from the oceanic middle latitudes, between Australia and New Zealand,
535 imprint of warm and wet air masses. When air masses in the free troposphere reach the
536 Antarctic continent, they are uplifted and temperature decreases by more than 50 K (not
537 shown). Note the air parcel at 400 hPa that is firstly originated from oceanic high latitudes in
538 the vicinity of the Antarctic continent but moves towards the middle oceanic latitudes with a
539 net subsidence and an increase of temperature of 30 K.

540 Regarding the diamond-dust period, Figure 15 (top right) shows the 5-day back-trajectories
541 at the 5 selected pressure levels on 5 April 2011 at 12:00 UTC corresponding to the time of
542 minimum temperature and absolute humidity of an air parcel issued from Dome C. We can
543 note that all the calculated air masses are originated from the Antarctic plateau whatever the
544 pressure level considered. Consequently, as already studied in Ricaud et al. (2012 and 2014c),
545 we thus expect that both temperature and H_2O tends to decrease on 5 April at 12:00 UTC

Atmos. Chem. Phys. Discuss., doi:10.5194/acp-2016-815, 2016
Manuscript under review for journal Atmos. Chem. Phys.
Published: 15 September 2016

compared to the surrounding periods because air masses with continental origins produce a cold and dry atmosphere above Dome C (as on 5 April 2011).

For episode 2, Figure 15 bottom left shows the 5-day back-trajectories at the 4 selected pressure levels of 650, 600, 500 and 400 hPa during the warm and wet period (see section 4) on 4 March 2013 at 08:00 UTC corresponding to the time of maximum temperature and absolute humidity of an air parcel issued from Dome C. At 650 hPa, the air parcel has a continental origin but migrates very close to the coast 2 days before reaching Dome C. Above, at 600, 500 and 400 hPa, all the air masses are coming from the oceanic middle-high latitudes ranging from 47°S to 63°S and from the surface to ~680 hPa, namely imprint of warm and wet air masses. As for episode 1, when air parcels in the free troposphere reach the Antarctic continent, they are uplifted and temperature decreases by 20-30 K (not shown). On 5 March at 18:00 UTC (Fig. 15 bottom right) during the cold and dry period of episode 2 corresponding to the time of minimum temperature and absolute humidity, the meteorological situation is radically different. Whatever the pressure level considered, the air parcels are all confined to the Antarctic plateau in the vicinity of the Dome C station, explaining again, as for episode 1, the cold and dry atmosphere observed during episode 2.

5.2. Integrated Water Vapour over Antarctica

If we consider the IWV fields as calculated by the NCEP/NCAR operational analyses (Kalnay et al., 1996) on 25 March 2011 and 5 April 2011 for the episode 1 over the Antarctic continent (Figure 16 top left and right, respectively), we obviously remark that the Eastern Antarctic plateau is much wetter on 25 March than on 5 April. The IWV calculated over the Dome C station is ~1.4 kg m^{-2} on 25 March 2011 and ~0.6 kg m^{-2} on 5 April 2011 in excellent agreement with the HAMSTRAD measurements (see section 3.2). This is indeed induced by the oceanic-origin flux bringing warm and wet air masses over the Dome C station on 25

Atmos. Chem. Phys. Discuss., doi:10.5194/acp-2016-815, 2016
Manuscript under review for journal Atmos. Chem. Phys.
Published: 15 September 2016

March and by the continent-origin flux bringing cold and dry air masses over the station on 5 April. The same exercise can be performed for the episode 2 (Figure 16 bottom left and right, respectively) considering the IWV fields as calculated by the NCEP/NCAR operational analyses on 4 and 5 March 2013. There, the IWV fields above Dome C show a similar pattern between 4 and 5 March but with a slight wet inflection on 4 March compared to 5 March with daily averaged values of ~0.6 and ~0.4 kg m^{-2}, respectively consistent with the daily-averaged values obtained at Dome C with HAMSTRAD (~0.55 and ~0.30 kg m^{-2}, respectively). Consequently, considering episodes 1 and 2, the thick-cloud episode observed during the warm and wet period above Dome C is attributed to air masses with an oceanic origin whilst the diamond dust episode occurring during the cold and dry period is attributed to air masses with continental origins.

5.3. Temperature and Water Vapour Budgets

We now intend to assess the tendency of temperature calculated by ARPEGE during episode 2 into radiation, turbulence, microphysics, and total advection and the tendency of water vapour into turbulence, microphysics, and total advection. Figure 17 shows the temperature budget calculated on 4 March 2013 over the warm and wet 12-h period 00:00-12:00 UTC and on 5 March 2013 over the dry and cold 12-h period 06:00-18:00 UTC whilst Figure 18 focuses on the water vapour budget.

For altitudes greater than ~100 m (3333 m amsl) above the ground on 4 March and greater than ~200 m on 5 March, the temperature tendency of the warm (Fig. 17 left) and of the cold (Fig. 17 right) periods is mainly dominated by the advection processes (red lines). This is fully consistent with the interpretation of the origin of air masses (previous subsection). Nevertheless, in the planetary boundary layer below approximately 100 m on 4 March and below 200 m on 5 March, the temperature tendency of the two periods is also governed by the

596 vertical mixing done by the turbulent processes (green line). Indeed, turbulence always tends
597 to stabilize the atmosphere impacted by radiative or dynamical forcing. The effect of the
598 radiative cooling on the surface temperature and its impact on the boundary layer is clearly
599 shown on 5 March (Fig. 17 right).

600 As for temperature, the water vapour tendency of the two periods also needs to be
601 separated at ~100 and ~200 m above the ground on 4 and 5 March, respectively. Above these
602 two limits, the water vapour tendency of the warm period (Fig. 18 left) and of the cold (Fig.
603 18 right) periods is governed by both the advection and the microphysical processes. On 4
604 March, a warmer and more humid air is advected (total water vapour tendency on Fig. 18 left
605 and total temperature advection on Fig. 17 left are positive), so the microphysics tend to
606 create some clouds by condensation (negative microphysics tendency, blue line on Fig. 18
607 left) with small precipitations close to the surface (~18 mm in 12 hours, not shown). On 5
608 March (Fig. 18 right), the water vapour advection (red line) is negative so a drier air is
609 advected toward the Dome C station. Below ~200 m, advection, turbulence and microphysical
610 (precipitation) processes compete to dehydrate the planetary boundary layer.

611 In general, this reinforces our conclusions of thick cloud episodes driven by warm and wet
612 air masses of oceanic origin and of diamond dust episodes driven by cold and dry air masses
613 of continental origin. Nevertheless, in the planetary boundary layer below approximately
614 ~100-200 m, the water vapour tendency of the two periods is competing between advection,
615 microphysical and turbulence processes.

616

617 ## 6. Conclusions

618 The present study takes the opportunity of combining several measurements and model
619 outputs to study the short-term evolution of the Antarctic atmosphere above the Dome C
620 station focusing on episodes of thick cloud and diamond dust. From 15 March to 8 April 2011

Atmos. Chem. Phys. Discuss., doi:10.5194/acp-2016-815, 2016
Manuscript under review for journal Atmos. Chem. Phys.
Published: 15 September 2016

and from 4 to 5 March 2013, the atmosphere has been probed by several instruments. 1) A ground-based microwave radiometer (HAMSTRAD) installed at Dome C that provided vertical profiles of tropospheric temperature and absolute humidity to calculate Integrated Water Vapour (IWV) with a 7-min integration time. 2) Daily radiosoundings launched at 12:00 UTC at Dome C. 3) A tropospheric aerosol Lidar that provides aerosol depolarization ratio along the vertical at Dome C. 4) Down- and upward short- and longwave radiations from an instrument installed at Dome C belonging to the BSRN network. 5) Space-borne aerosol depolarization ratio from the CALIOP Lidar aboard the CALIPSO platform along orbits close to the Dome C station.

The time evolution of the atmosphere over the 1-month period in 2011 has also been evaluated by considering the outputs from the mesoscale model AROME in 3 configurations. 1) “Operational”, operating mode with a snow albedo of 0.80. 2) “Operational with ice tuning”, as in “Operational” but with a setting of snow albedo that can reach up to 0.85. And finally 3) “ARPEGE micro-physics”, as in “Operational with ice tuning” but includes the physics of ARPEGE and a state-of-the-art scheme to represent the snow pattern taking into account the roughness length. The ARPEGE global-scale meteorological model analyses gave the state of the atmosphere and relevant prognostics (ice precipitation, temperature and water vapour budget) on 4 and 5 March 2013.

Two distinct periods are highlighted by all the datasets: the warm and wet periods (24-26 March 2011 and 4 March 2013) and the cold and dry periods (5 April 2011 and 5 March 2013). Although the time evolution of temperature in the planetary boundary layer and in the free troposphere is consistent within all the data sets, AROME in 2011 tends to model a warmer atmosphere during these two specific events at 4 m. The time evolution of absolute humidity is also consistent within all the data sets with some known wet bias in HAMSTRAD compared to radiosondes in the planetary boundary layer, and with some systematic wet bias

of AROME compare to radiosondes. In general, IWV from HAMSTRAD and radiosondes are consistent with each other although AROME tends to be much wetter than the two measurements. ARPEGE analyses in 2013, consistently with HAMSTRAD data, reproduce the warm and wet period, and the cold and dry period.

Since the longwave radiations (both downward and upward) are much greater than the shortwave radiations (both downward and upward) during the warm and wet period of 2011, the effect is that the net irradiance is positive or close to zero. This obviously indicates that a thick cloud is shielding the downward shortwave radiation (coming from the Sun) and increases the downward longwave radiation (coming from the cloud). During the cold and dry periods, there is not an abrupt increase of longwave downward radiation but the downward shortwave radiation is only slightly greater than the upward shortwave radiation, and the net irradiance does not exhibit an obvious diurnal cycle maximizing at local noon. Consequently, both the shortwave and the total irradiance analyses tend to suggest the presence of a cloud.

Considering upward and downward active measurements of aerosols from two Lidars installed at Dome C and aboard a spaceborne platform, respectively, the signature of a thick cloud with high depolarization ratios (greater than 30%) is detected during the warm and wet periods from the surface to ~5-7 km with precipitation of ice particles and the presence of a supercooled liquid water cloud with low depolarization ratios (~10%). During the cold and dry periods, high depolarization ratios (greater than 30%) to a maximum height of 100-500 m is measured suggesting that the cloud is constituted of ice crystals with no trace of precipitation. This means ice crystals are in suspension in the air. This case is usually referred to as “diamond dust”.

The presence of a thick cloud during the warm and wet period of 2011 is calculated by the 2D nebulosity fields from AROME extending from the ground to ~6 km altitude with values greater in the micro-physics run than in the two other configurations. In the three

configurations, high nebulosity values (greater than 0.8) are calculated close to the surface (0-200 m), almost systematically in the two first configurations (operational and operational with ice tuning). The AROME model tends to produce a sort of cloud residual in the planetary boundary layer in the three configurations analyzed so the presence of a thin cloud close to the surface cannot be ruled out. The thick-cloud episode during the warm and wet period of 2013 is well reproduced by ARPEGE together with the ice precipitation but the diamond dust episode cannot be calculated during the cold and dry episode. No liquid water clouds are estimated by the ARPEGE analyses.

Considering 5-day back trajectories from Dome C and global distributions of IWV over the Antarctic in 2011 and 2013 tends to show that the thick-cloud episodes observed during the warm and wet periods above Dome C can be attributed to air masses with an oceanic origin whilst the diamond dust episode occurring during the cold and dry periods can be attributed to air masses with continental origins. This is confirmed by the ARPEGE temperature tendencies calculated during the warm and the cold periods of 2013 that are mainly dominated by the advection components whilst the water vapour tendencies are governed by both the advection and the microphysical processes.

The analysis of these two periods is going to be enlarged towards a climatological survey of the presence of clouds and of their types above the Dome C station during the period 2009-2016. We will combine measurements from the same instruments and outputs from the same model together with new instruments installed at the station providing the microphysical and optical properties of the ice crystals that deposit at the surface.

Acknowledgment

The present research project HAMSTRAD programme (910) has been performed at the Dome C station and was supported by the French Polar Intitute, Institut polaire français Paul-

696 Emile Victor (IPEV), the Institut National des Sciences de l'Univers (INSU)/Centre National
697 de la Recherche Scientifique (CNRS), Météo-France and the Centre National d'Etudes
698 Spatiales (CNES). The permanently manned Concordia station is jointly operated by IPEV
699 and the Italian Programma Nazionale Ricerche in Antartide (PNRA). We would like to thank
700 all the winterover personels who worked at Dome C on the different projects: HAMSTRAD,
701 Routine Meteorological Observations (RMO), aerosol Lidar and BSRN. Thanks to the British
702 Atmospheric Data Centre, which is part of the Natural Environment Research Council
703 (NERC) National Centre for Atmospheric Science (NCAS), for the calculation of trajectories
704 and access to European Centre for Medium-Range Weather Forecasts (ECMWF) data. We
705 have used NCEP Reanalysis data provided by the NOAA/OAR/ESRL PSD, Boulder,
706 Colorado, USA, from their Web site at http://www.esrl.noaa.gov/psd/. The authors also would
707 like to thank the CALIPSO science team for providing the CALIOP images at http://www-
708 calipso.larc.nasa.gov/. HAMSTRAD data are available at
709 http://www.cnrm.meteo.fr/spip.php?article961&lang=en. RMO data are available at
710 http://www.climantartide.it
711
712

712 **References**

713 Adhikari, L., Wang, Z. and Deng, M.: Seasonal variations of Antarctic clouds observed by
714 CloudSat and CALIPSO satellites, J. Geophys. Res., 117, D04202,
715 doi:10.1029/2011JD016719, 2012.
716 Argentini, S., Viola, A., Sempreviva, A. M. and Petenko, I.: Summer boundary-layer height at
717 the plateau site of Dome C, Antarctica, Bound.-Layer Meteor., 115, 409-422, 2005.
718 Bailey, M. P., and Hallett, J: A comprehensive habit diagram for atmospheric ice crystals:
719 Confirmation from the laboratory, AIRS II, and other field studies, J. Atmos. Sci., 66,
720 2888-2899, 2009.
721 Bazile, E., Marquet, P., Bouteloup, Y., and Bouyssel, F.: The Turbulent Kinetic Energy
722 (TKE) scheme in the NWP models at Météo-France, ECMWF Proceedings "Workshop on
723 Diurnal cycles and the stable boundary layer", 127-136, 2011.
724 Bosveld, F. C., Baas, P., Steeneveld, G. J., Holtslag, A. A., Angevine, W. M., Bazile, E., de
725 Bruijn, E. I. F., Deacu, D., Edwards, J. M., Ek, M., Larson, V. E., Pleim, J. E.,
726 Raschendorfer, M. and Svensson, G.: The third GABLS intercomparison case for
727 evaluation studies of boundary-layer models. Part B: results and process understanding,
728 Bound.-Layer Meteor., 152, 157-187, 2014.
729 Bouteloup, Y., Bouyssel, F., and Marquet, P.: Improvements of Lopez's progonostic large
730 scale cloud and precipitation scheme, ALADIN Newsletter, 28, 66-73, 2005.
731 Brasseur, G. P., Orlando, J. J., and Tyndall, G. S.: Atmospheric chemistry and global change,
732 2nd edition, Oxford University Press, New York, Oxford, ISBN-0-19-510521-4, 1999.
733 Davis, D., Nowak J. B., Chen G., Buhr M., Arimoto R., Hogan A., Eisele F., Mauldin L.,
734 Tanner D., Shetter R., Lefer B., and McMurry P.: Unexpected high levels of NO observed
735 at South Pole, Geophys. Res. Lett., 28, 3625-3628, 2001.

736 Douville, H., Royer, J.-F. and Mahfouf, J.-F.: A new snow parameterization for the Météo-
737 France climate model, Part I : Validation in stand-alone experiments, Clim. Dynam., 12,
738 21-35, 1995.
739 Dufresne, J. L. and Bony, S.: An assessment of the primary sources of spread of global
740 warming estimates from coupled atmosphere-ocean models, J. Climate, 21, 5135-5144,
741 2008.
742 Fouquart, Y., and Bonnel, B.: Computations of solar heating of the earth's atmosphere: a new
743 parameterization, Beitr. Phys. Atmosph., 53, 35-62, 1980.
744 Hines, K. M., Bromwich, D. H., Rasch, P. J. and Iacono, M. J.: Antarctic clouds and radiation
745 within the NCAR climate models, J. Climate, 17, 1198–1212, doi:10.1175/1520-
746 0442(2004)017, 2004.
747 Hudson, S. R., Warren, S. G., Brandt, R. E., Grenfell, T. C., and Six, D.: Spectral
748 bidirectional reflectance of Antarctic snow: Measurements and parameterization, J.
749 Geophys. Res., 111, D18106, doi:10.1029/2006JD007290, 2006.
750 Kalnay, E., Kanamitsu, M., Kistler, R., Collins, W., Deaven, D., Gandin, L., Iredell, M., Saha,
751 S., White, G., Woollen, J., Zhu, Y., Leetmaa, A., Reynolds, R., Chelliah, M., Ebisuzaki,
752 W., Higgins, W. Janowiak, J., Mo, K. C., Ropelewski, C., Wang, J., Jenne, R. and Dennis
753 Joseph, D.: The NCEP/NCAR 40-Year Reanalysis Project, Bull. Amer. Meteor. Soc., 77,
754 437–471, 1996.
755 Lanconelli, C., Busetto, M., Dutton, E. G., König-Langlo, G., Maturilli, M., Sieger, R., Vitale,
756 V. and Yamanouchi, T.: Polar baseline surface radiation measurements during the
757 International Polar Year 2007-2009: Earth System Science Data, 3(1), 1-8,
758 doi:10.5194/essd-3-1-2011, 2011.

759 Lawson, R. P., Baker, B. A., Zmarzly, P., O'Connor, D., Mo, Q., Gayet, J. F. and
760 Shcherbakov, V.: Microphysical and optical properties of atmospheric ice crystals at
761 South Pole Station, J. Appl. Meteor., 45, 1505-1524, 2006.
762 Lindqvist, H., Muinonen, K., Nousiainen, T., Um, J., McFarquhar, G. M., Haapanala, P.,
763 Makkonen, R. and Hakkarainen, H.: Ice-cloud particle habit classification using principal
764 components, J. Geophys. Res., 117, D16206, doi:10.1029/2012JD017573, 2012.
765 Lopez, P.: Implementation and validation of a new prognostic large-scale cloud and
766 precipitation scheme for climate and data assimilation purposes, Q. J. R. Meteorol. Soc.,
767 128, 229-257, 2002.
768 Lubin, D., Chen, B., Bromwich, D. H., Somerville, R. C., Lee, W. H., and Hines, K. M.: The
769 Impact of Antarctic Cloud Radiative Properties on a GCM Climate Simulation, J. Climate,
770 11, 447-462, 1998.
771 Miloshevich, L. M., Vömel, H., Whiteman, D. N., Lesht, B. M., Schmidlin, F. J. and Russo,
772 F.: Absolute accuracy of water vapor measurements from six operational radiosonde types
773 launched during AWEX-G and implications for AIRS validation, J. Geophys. Res., 111,
774 D09S10, doi:10.1029/2005JD006083, 2006.
775 Miloshevich, L. M., Vömel, H., Whiteman, D. N. and Leblanc, T.: Accuracy assessment and
776 corrections of Vaisala RS92 radiosonde water vapour measurements, J. Geophys. Res.,
777 114, D11305, doi:10.1029/2008JD011565, 2009.
778 Mishchenko, M. I., J. W. Hovenier, and L. D. Travis (Eds.): Light Scattering by Nonspherical
779 Particles: Theory, Measurements, and Applications. Academic Press. Chapter 14, 393-
780 416, 2000.
781 Mlawer, E. J., Taubman, S. J., Brown, P. D., Iacono, M. J. and Clough, S. A.: Radiative
782 transfer for inhomogeneous atmospheres: RRTM, a validated correlated-k model for the
783 longwave, J. Geophys. Res., 102D, 16663-16682, 1997.

784 Morcrette, J.-J., Mlawer, E. J., Iacono, M. J. and Clough, S. A.: Impact of the radiation
785 transfer scheme RRTM in the ECMWF forecasting system, ECMWF Newsletter, 91, 2-9,
786 2001.
787 Palchetti, L., Bianchini, G., Di Natale, G., and Del Guasta, M.: Far infrared radiative
788 properties of water vapor and clouds in Antarctica, B. Am. Meteorol. Soc., 96, 1505-1518,
789 doi:10.1175/BAMS-D-13-00286.1, 2015
790 Pirazzini, R.: Surface albedo measurements over Antarctic sites in summer, J. Geophys. Res.,
791 109, D20118, doi:10.1029/2004JD004617, 2004.
792 Ricaud, P., Gabard, B., Derrien, S., Chaboureau, J.-P., Rose, T., Mombauer, A. and Czekala,
793 H.: HAMSTRAD-Tropo, A 183-GHz Radiometer Dedicated to Sound Tropospheric
794 Water Vapor Over Concordia Station, Antarctica, IEEE Trans Geosci Remote Sens., 48,
795 1365–1380, doi: 10.1109/TGRS.2009.2029345, 2010.
796 Ricaud, P., Genthon, C., Durand, P., Attié, J.-L., Carminati, F., Canut, G., Vanacker, J.-F.,
797 Moggio, L., Courcoux, Y., Pellegrini, A. and Rose, T.: Summer to Winter Diurnal
798 Variabilities of Temperature and Water Vapor in the lowermost troposphere as observed
799 by the HAMSTRAD Radiometer over Dome C, Antarctica, Bound.-Layer Meteor., 143,
800 227–259, doi:10.1007/s10546-011-9673-6, 2012.
801 Ricaud, P., Carminati, F., Attié, J.-L., Courcoux, Y., Rose, T., Genthon, C., Pellegrini, A.,
802 Tremblin, P. and August, T: Quality Assessment of the First Measurements of
803 Tropospheric Water Vapor and Temperature by the HAMSTRAD Radiometer over
804 Concordia Station, Antarctica, IEEE Trans Geosci Remote Sens., 51, 3217–3239, doi:
805 10.1109/TGRS.2012.2225627, 2013.
806 Ricaud, P., Carminati, F., Courcoux, Y., Pellegrini, A., Attié, J.-L., El Amraoui, L., Abida, R.,
807 Genthon, C., August, T. and Warner, J.: Statistical Analyses and Correlation between

808 Tropospheric Temperature and Humidity at Dome C, Antarctica, Antarct. Sci., 26, 290 –
809 308. doi:10.1017/S0954102013000564, 2014a.
810 Ricaud, P.: Variabilités de la vapeur d'eau et de la température troposphérique au Dôme C
811 (station Concordia), Antarctique. Partie I : l'instrument Hamstrad, La Météorologie, 84,
812 15-28, doi:10.4267/2042/53184, 2014b.
813 Ricaud, P.: Variabilités de la vapeur d'eau et de la température troposphérique mesurées par
814 le radiomètre micro-onde HAMSTRAD au Dôme C, Antarctique. Partie II : Résultats
815 scientifiques, La Météorologie, 85, 35-46, doi:10.4267/2042/53749, 2014c.
816 Ricaud, P., Grigioni, P., Zbinden, R., Attié, J.-L., Genoni, L., Galeandro, A., Moggio, A.,
817 Montaguti, S., Petenko, I. and Legovini, P.: Review of tropospheric temperature, absolute
818 humidity and integrated water vapour from the HAMSTRAD radiometer installed at
819 Dome C, Antarctica, 2009–14, Antarct. Sci., 27, 598-616,
820 doi:10.1017/S0954102015000334, 2015.
821 Seity, Y., Brousseau, P., Malardel, S., Hello, G., Bénard, P., Bouttier, F., Lac, C. and Masson,
822 V.: The AROME-France Convective-Scale Operational Model, Mon. Wea. Rev., 139,
823 976–991, 2011.
824 Tomasi, C., B. Petkov, E. Benedetti, V. Vitale, A. Pellegrini, G. Dargaud, L. De Silvestri, P.
825 Grigioni, E. Fossat, W.L. Roth, and L. Valenziano: Characterization of the atmospheric
826 temperature and moisture conditions above Dome C (Antarctica) during austral summer
827 and fall months, J. Geophys. Res., lll, D20305, doi:10.1029/2005jD006976, 2006.
828 Tomasi, C., Petkov, B., Benedetti, E., Valenziano, L. and Vitale, V.: Analysis of a 4 year
829 radiosonde dataset at Dome C for characterizing temperature and moisture conditions of
830 the Antarctic atmosphere, J. Geophys. Res., 116, D15304, doi:10.1029/2011JD015803,
831 2011.

832 Tomasi, C., Petkov, B. H. and Benedetti, E.: Annual cycles of pressure, temperature, absolute
833 humidity and precipitable water from the radiosoundings performed at Dome C,
834 Antarctica, over the 2005-2009 period, Antarct. Sci., 24, 637–658,
835 doi:10.1017/S0954102012000405, 2012.
836 Tremblin, P., V. Minier, N. Schneider, G. Al. Durand, M. C. B. Ashley, J. S. Lawrence, D. M.
837 Luong-van, J. W. V. Storey, G. An. Durand, Y. Reinert, C. Veyssiere, C. Walter, P.
838 Ade, P. G. Calisse, Z. Challita, E. Fossat, L. Sabbatini, A. Pellegrini, P. Ricaud and J.
839 Urban: Site testing for submillimetre astronomy at Dome C in Antarctica, Astronomy
840 and Astrophysics, 535 A112, DOI: http://dx.doi.org/10.1051/0004-6361/201117345,
841 2011.
842 Turner, J., Lachlan-Cope, T. A., Colwell, S., Marshall, G. J. and Connolley, W. M.:
843 Significant Warming of the Antarctic Winter Troposphere, Science, 311,
844 doi:10.1126/science.1121652, 2006.
845 Walden, V. P., Warren, S. G. and Tuttle, E.: Atmospheric ice crystals over the Antarctic
846 Plateau in winter, J. Appl. Meteorol., 42, 1391-1405, 2003.
847 Winker, D. M., Vaughan, M. A., Omar, A., Hu, Y., Powell, K. A., Liu, Z., Hunt, W. H. and
848 Young, S. A.: Overview of the CALIPSO mission and CALIOP data processing
849 algorithms, J. Atmos. Oceanic Technol., 26, 2310-2323, 2009.
850 Young, S. A. and Vaughan, M. A.: The retrieval of profiles of particulate extinction from
851 Cloud Aerosol Lidar Infrared Pathfinder Satellite Observations (CALIPSO) lidar data:
852 Algorithm description, J. Atmos. Oceanic Technol., 26, 1105–1119, 2009.
853

Atmos. Chem. Phys. Discuss., doi:10.5194/acp-2016-815, 2016
Manuscript under review for journal Atmos. Chem. Phys.
Published: 15 September 2016

Atmospheric Chemistry and Physics Discussions

853 **Figure Caption**

854

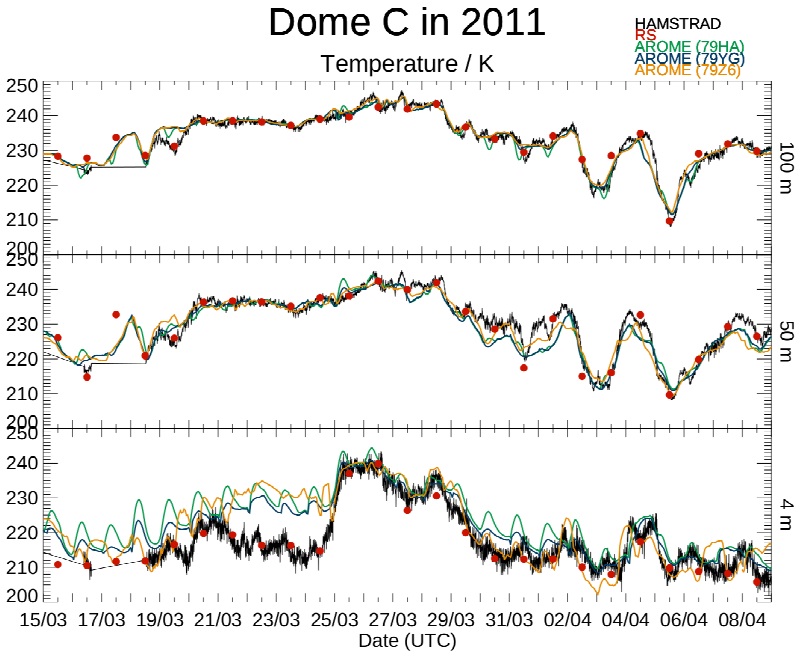

855
856
857 **Fig. 1:** From bottom to top: Time evolution of temperature from 15 March to 8 April 2011
858 above Dome C as measured by the HAMSTRAD radiometer (black line), the radiosondes (red
859 filled circles), and as calculated by the mesoscale model AROME according to different runs:
860 a) operational (green line), b) operational with ice tuning (blue line) and c) considering
861 ARPEGE micro-physics (orange line) at 4, 50 and 100 m.

862
863
864

Atmos. Chem. Phys. Discuss., doi:10.5194/acp-2016-815, 2016
Manuscript under review for journal Atmos. Chem. Phys.
Published: 15 September 2016

Atmospheric Chemistry and Physics Discussions

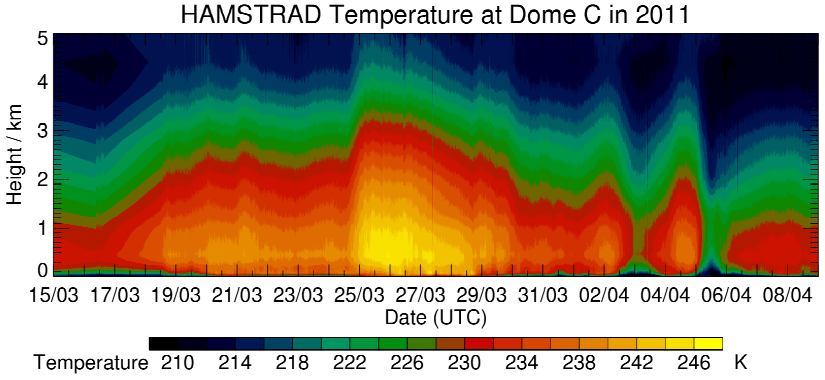

Fig. 2: Time evolution of temperature from 15 March to 8 April 2011 above Dome C as measured by the HAMSTRAD radiometer from 0 to 5 km.

Atmos. Chem. Phys. Discuss., doi:10.5194/acp-2016-815, 2016
Manuscript under review for journal Atmos. Chem. Phys.
Published: 15 September 2016

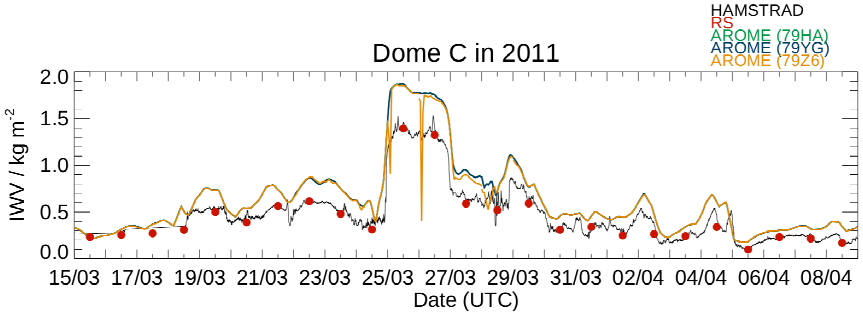

Fig. 3: Time evolution of IWV from 15 March to 8 April 2011 above Dome C as measured by the HAMSTRAD radiometer (black line), the radiosondes (red filled circles), and as calculated by the mesoscale model AROME according to different runs: a) operational (green line), b) operational with ice tuning (blue line) and c) considering ARPEGE micro-physics (orange line).

Atmos. Chem. Phys. Discuss., doi:10.5194/acp-2016-815, 2016
Manuscript under review for journal Atmos. Chem. Phys.
Published: 15 September 2016

Atmospheric Chemistry and Physics Discussions

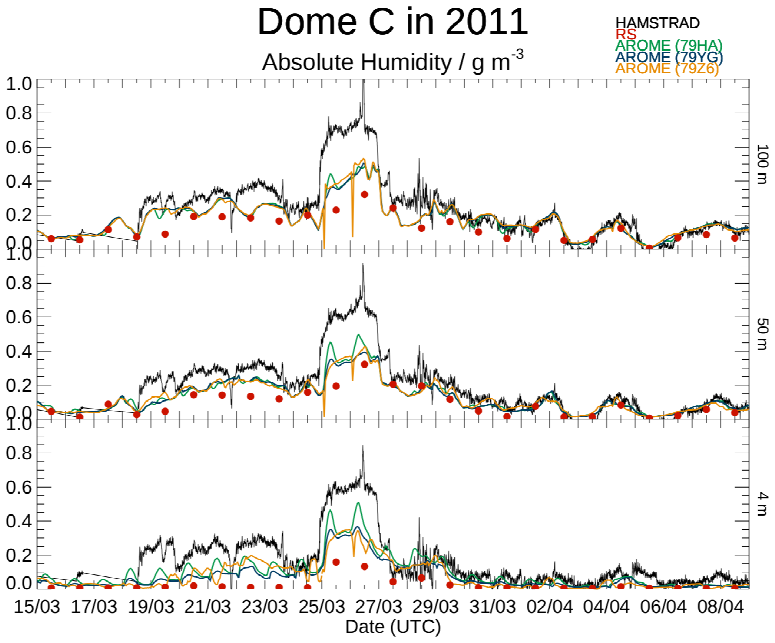

874
875
876 **Fig. 4:** From bottom to top: Time evolution of absolute humidity from 15 March to 8 April
877 2011 above Dome C as measured by the HAMSTRAD radiometer (black line), the
878 radiosondes (red filled circles), and as calculated by the mesoscale model AROME according
879 to different runs: a) operational (green line), b) operational with ice tuning (blue line) and c)
880 considering ARPEGE micro-physics (orange line) at 4, 50 and 100 m.
881

Atmos. Chem. Phys. Discuss., doi:10.5194/acp-2016-815, 2016
Manuscript under review for journal Atmos. Chem. Phys.
Published: 15 September 2016

Atmospheric Chemistry and Physics Discussions

881

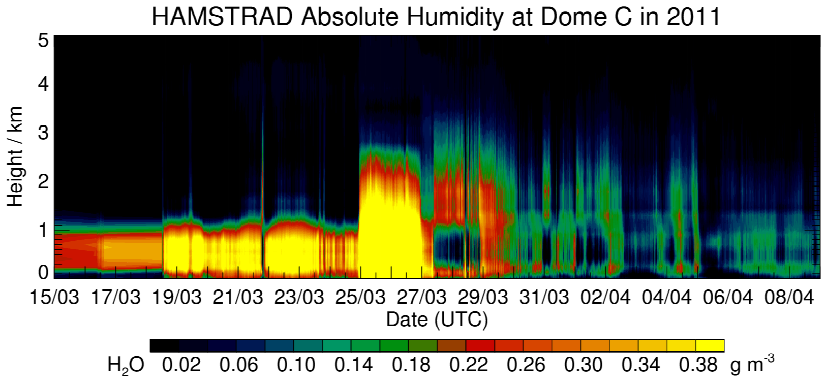

882

883 **Fig. 5:** Time evolution of absolute humidity from 15 March to 8 April 2011 above Dome C as

884 measured by the HAMSTRAD radiometer from 0 to 5 km.

885

886

Atmos. Chem. Phys. Discuss., doi:10.5194/acp-2016-815, 2016
Manuscript under review for journal Atmos. Chem. Phys.
Published: 15 September 2016

Atmospheric Chemistry and Physics Discussions

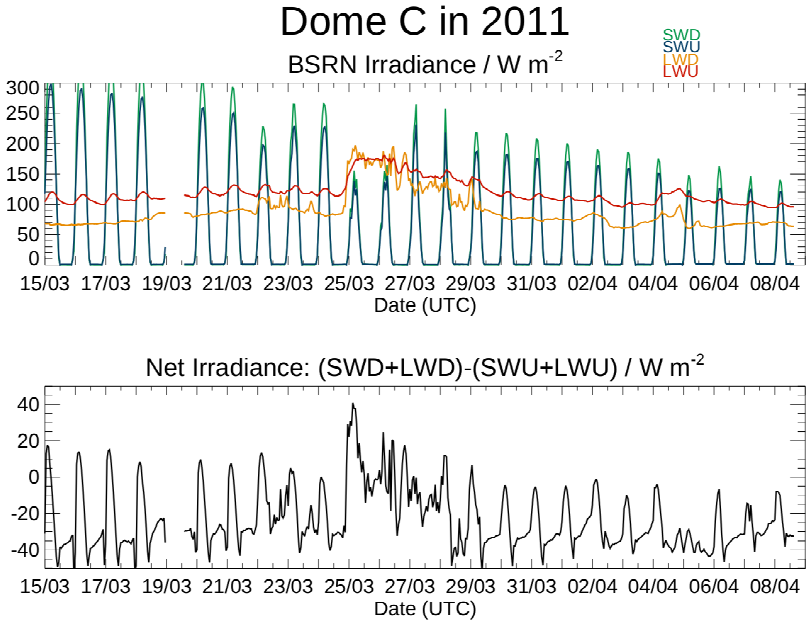

886

887 **Fig. 6:** (Top) Time evolution of downward shortwave radiation (SWD, green line), upward
888 shortwave radiation (SWU, blue line), downward longwave radiation (LWD, orange line),
889 and upward longwave radiation (LWU, red line) from 15 March to 8 April 2011 above Dome
890 C as measured by the BSRN instruments. (Bottom) Net irradiance (SWD+LWD-SWU-
891 LWU) as measured by the BSRN instruments.

892

Atmos. Chem. Phys. Discuss., doi:10.5194/acp-2016-815, 2016
Manuscript under review for journal Atmos. Chem. Phys.
Published: 15 September 2016

Atmospheric Chemistry and Physics Discussions

892

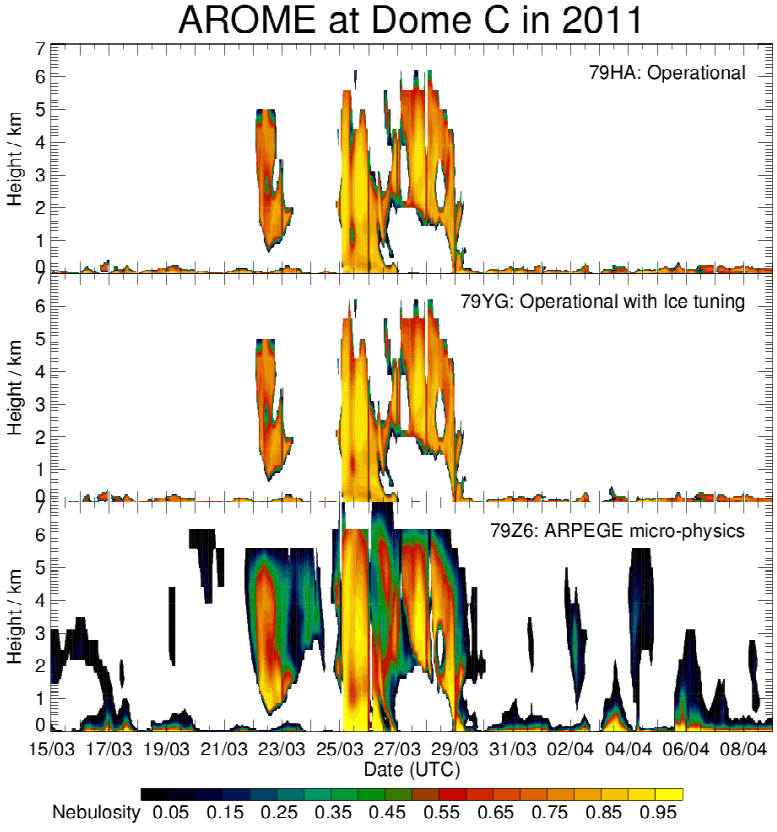

893
894
895 **Fig. 7:** (From top to bottom) Time evolution of nebulosity from 15 March to 8 April 2011
896 above Dome C as calculated by the mesoscale model AROME according to different runs:
897 operational (top), operational with ice tuning (center) and considering ARPEGE micro-
898 physics (bottom). See the text for further information regarding the AROME runs.
899

Atmos. Chem. Phys. Discuss., doi:10.5194/acp-2016-815, 2016
Manuscript under review for journal Atmos. Chem. Phys.
Published: 15 September 2016

Atmospheric Chemistry and Physics Discussions

899

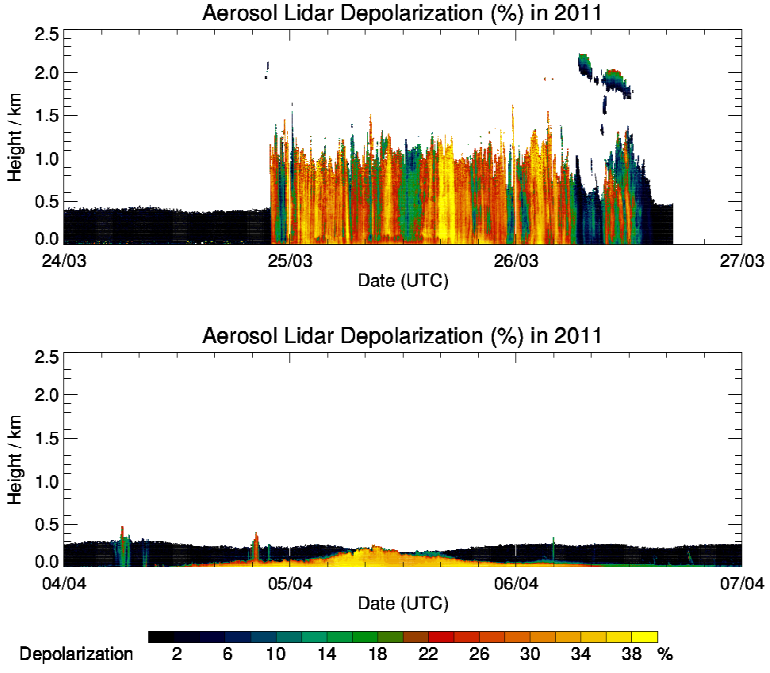

900
901 **Fig. 8:** (Top, from left to right) Aerosol depolarization as measured by the Lidar installed at
902 the Dome C station over the period 24-26 March 2011. (Bottom, from left to right) Aerosol
903 depolarization as measured by the Lidar installed at the Dome C station over the period 4-6
904 April 2011.

905

906

Atmos. Chem. Phys. Discuss., doi:10.5194/acp-2016-815, 2016
Manuscript under review for journal Atmos. Chem. Phys.
Published: 15 September 2016

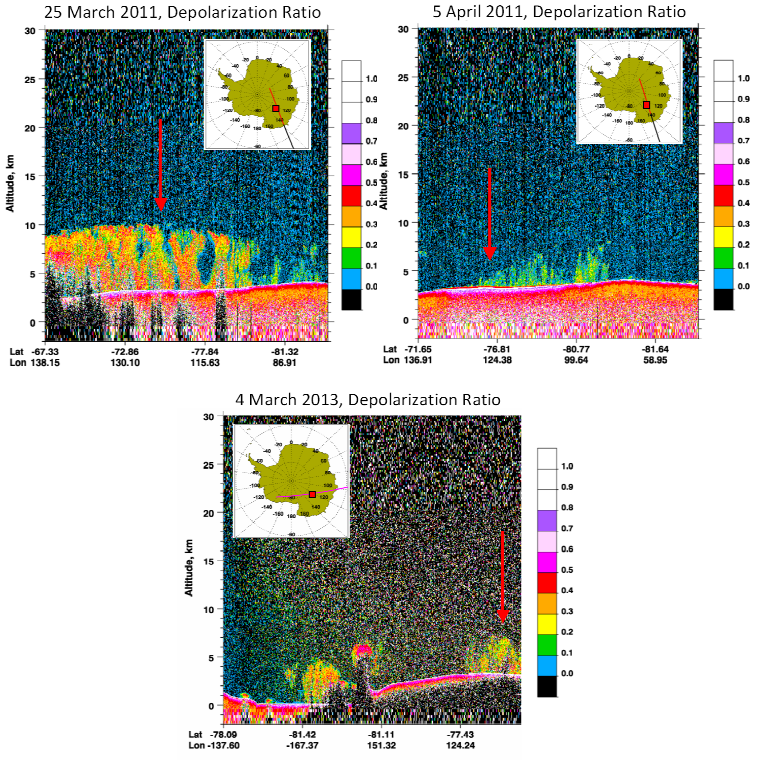

906

907

908 **Fig. 9:** Spaceborne Lidar CALIOP measurements of depolarization ratio along one orbit in
909 the vicinity of the Dome C station on 25 March 2011 (top left), 5 April 2011 (top right) and 4
910 March 2013 (bottom). The red square represents the location of the Dome C station. The red
911 vertical arrow represents the approximate location of the Dome C station.

912

913

Atmos. Chem. Phys. Discuss., doi:10.5194/acp-2016-815, 2016
Manuscript under review for journal Atmos. Chem. Phys.
Published: 15 September 2016

Atmospheric Chemistry and Physics Discussions

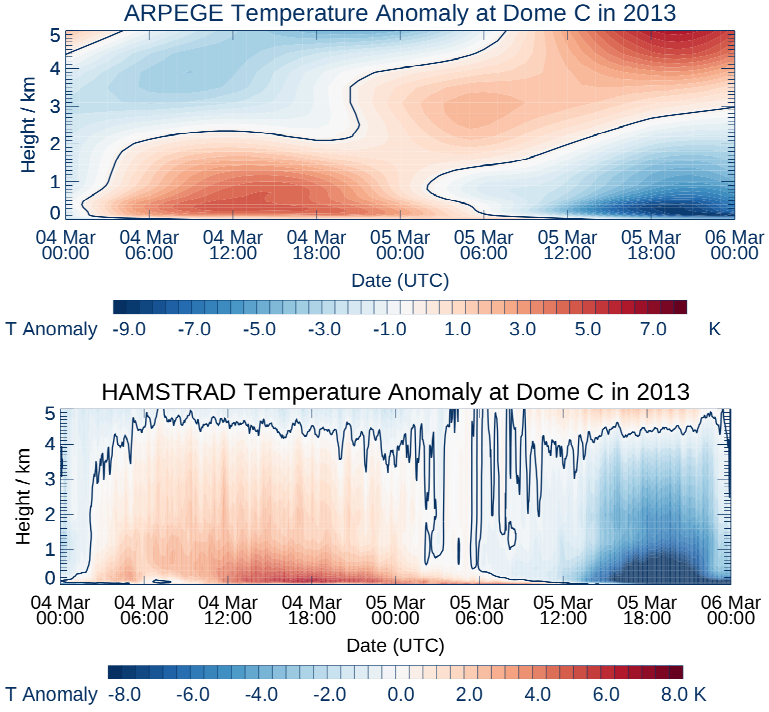

Fig. 10: Temperature anomaly from 4 to 5 March 2013 above the Dome C station as calculated by the ARPEGE model (top) and as measured by the HAMSTRAD radiometer (bottom).

Atmos. Chem. Phys. Discuss., doi:10.5194/acp-2016-815, 2016
Manuscript under review for journal Atmos. Chem. Phys.
Published: 15 September 2016

Atmospheric Chemistry and Physics Discussions

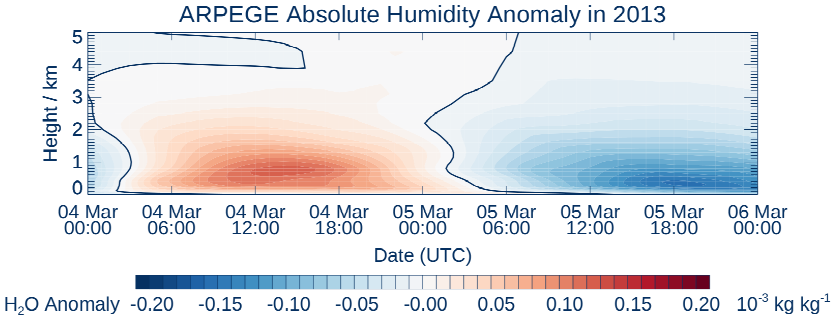

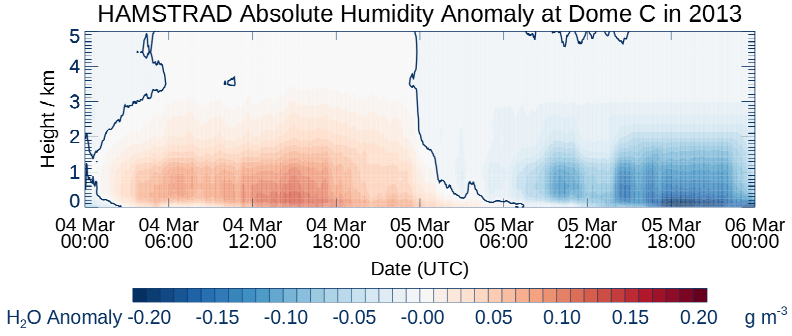

Fig. 11: Absolute Humidity anomaly from 4 to 5 March 2013 above the Dome C station as calculated by the ARPEGE model (top) and as measured by the HAMSTRAD radiometer (bottom).

Atmos. Chem. Phys. Discuss., doi:10.5194/acp-2016-815, 2016
Manuscript under review for journal Atmos. Chem. Phys.
Published: 15 September 2016

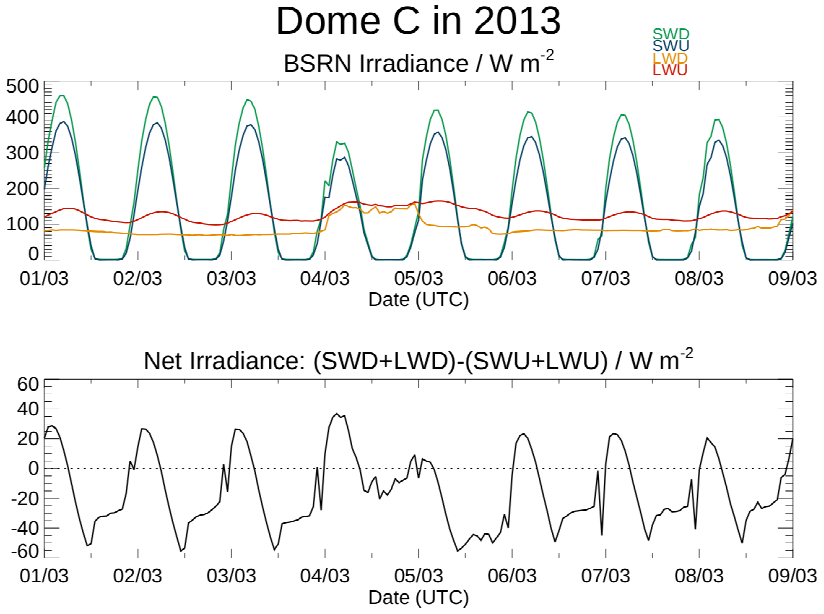

925

926 **Fig. 12:** (Top) Time evolution of downward shortwave radiation (SWD, green line), upward
927 shortwave radiation (SWU, blue line), downward longwave radiation (LWD, orange line),
928 and upward longwave radiation (LWU, red line) from 1 to 9 March 2013 above Dome C as
929 measured by the BSRN instruments. (Bottom) Net irradiance (SWD+LWD-SWU-LWU) as
930 measured by the BSRN instruments.

931

932

Atmos. Chem. Phys. Discuss., doi:10.5194/acp-2016-815, 2016
Manuscript under review for journal Atmos. Chem. Phys.
Published: 15 September 2016

Atmospheric Chemistry and Physics Discussions

932

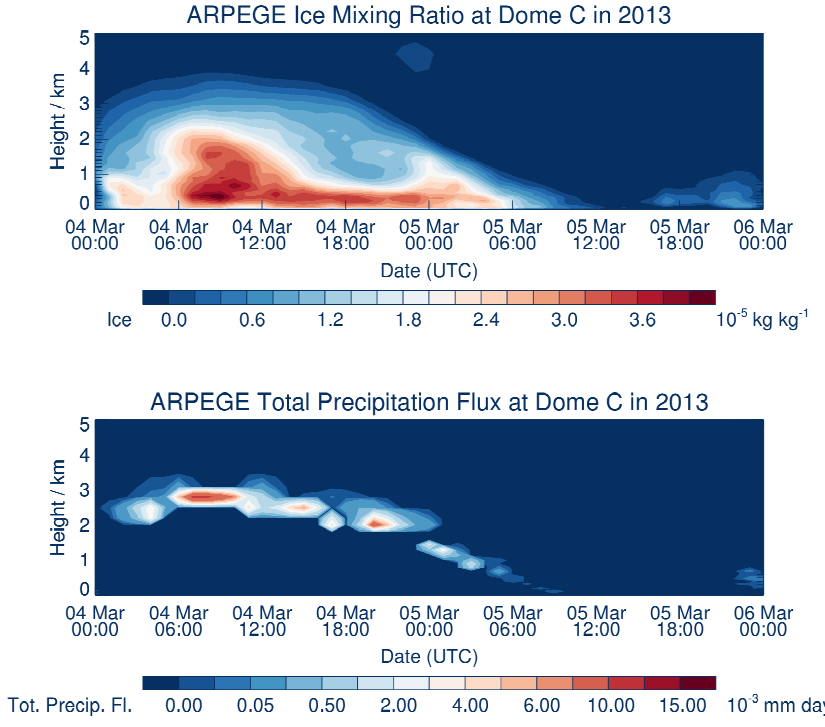

933

934

935 **Fig. 13:** Time evolution of the Ice Water Mixing ratio (top) and of the Total Precipitation
936 Flux (bottom) from 4 to 5 March 2013 above the Dome C station as calculated by the
937 ARPEGE model.

938

939

Atmos. Chem. Phys. Discuss., doi:10.5194/acp-2016-815, 2016
Manuscript under review for journal Atmos. Chem. Phys.
Published: 15 September 2016

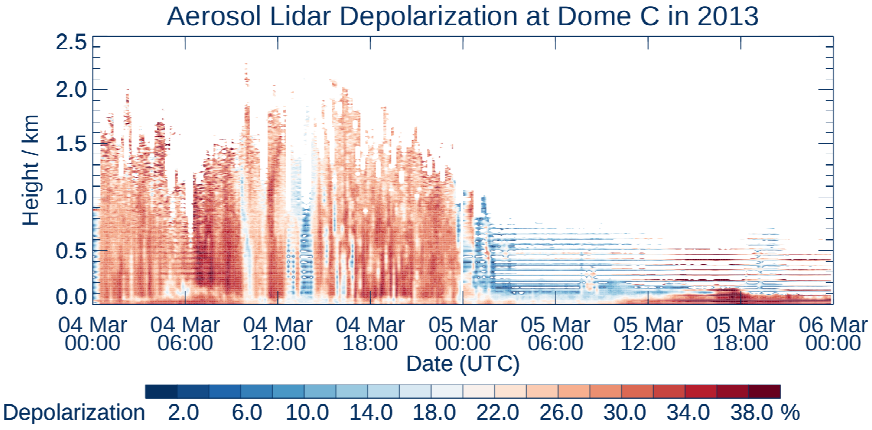

939

940 **Fig. 14:** Time evolution of the Depolarization ratio (%) from 4 to 5 March 2013 above the

941 Dome C station as measured by the aerosol Lidar installed at Dome C.

942

Atmos. Chem. Phys. Discuss., doi:10.5194/acp-2016-815, 2016
Manuscript under review for journal Atmos. Chem. Phys.
Published: 15 September 2016

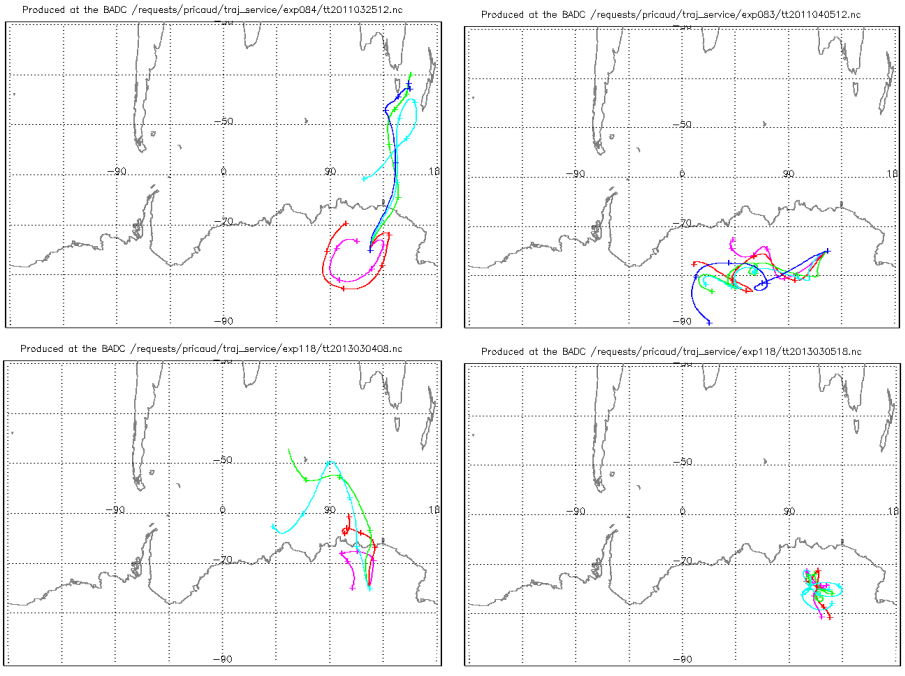

Fig. 15: (Top) Five-day back-trajectories of air masses originated from Dome C on 25 March 2011 at 12:00 UTC (left) and on 5 April 2011 at 12:00 UTC (right) at 650 (pink line), 600 (red line), 500 (green line), 400 (light blue line) and 300 hPa (dark blue line). (Bottom) Same as top but on 4 March 2013 at 08:00 UTC (left) and on 5 March 2013 at 18:00 UTC (right).

Atmos. Chem. Phys. Discuss., doi:10.5194/acp-2016-815, 2016
Manuscript under review for journal Atmos. Chem. Phys.
Published: 15 September 2016

Atmospheric Chemistry and Physics Discussions

952

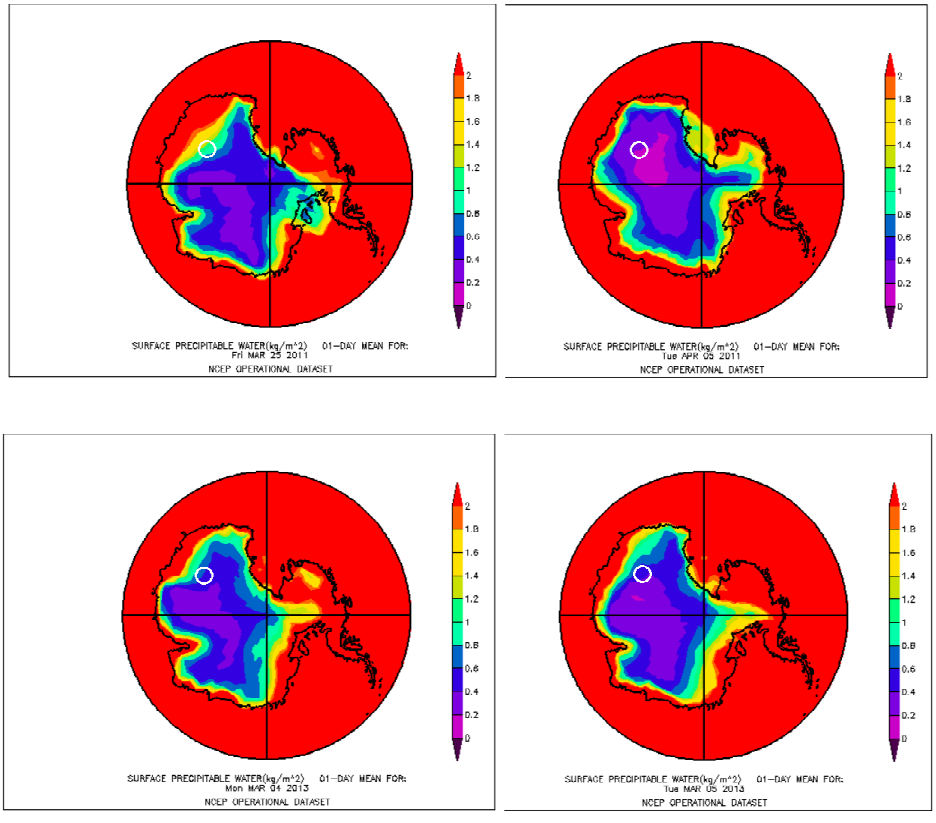

953

954 **Fig. 16:** IWV calculated above the Antarctic continent from the NCEP/NCAR operational
955 analyses on 25 March 2011 (top left), 5 April 2011 (top right), 4 March 2013 (bottom left)
956 and 5 March 2013 (bottom right). The white circle represents the position of the Dome C
957 station.

958

959

Atmos. Chem. Phys. Discuss., doi:10.5194/acp-2016-815, 2016
Manuscript under review for journal Atmos. Chem. Phys.
Published: 15 September 2016

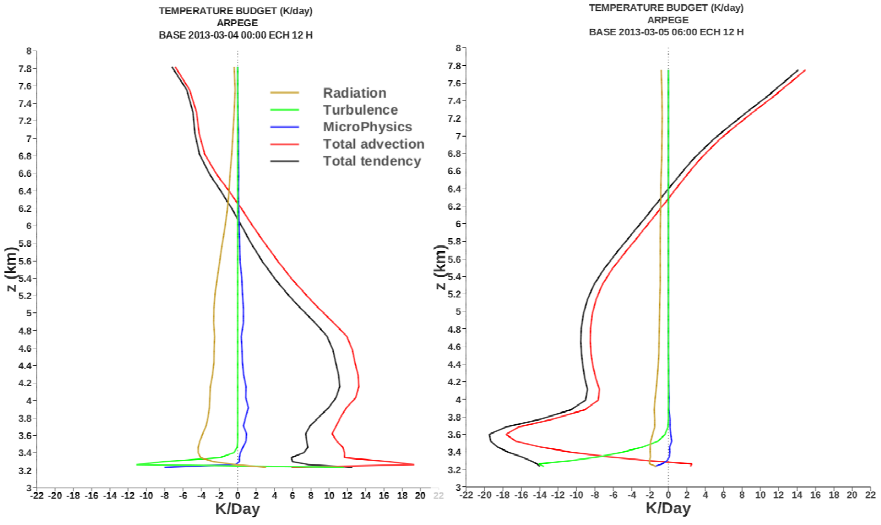

959

960 **Fig. 17:** (Left) Temperature budget calculated by ARPEGE on 4 March 2013 over the 12-h
961 period 00:00-12:00 UTC induced by radiation (brown), turbulence (green), microphysics
962 (blue), total advection (red) showing the total tendency (black). (Right) Same as Left but on 5
963 March 2013 over the 12-h period 06:00-18:00 UTC.

964

Atmos. Chem. Phys. Discuss., doi:10.5194/acp-2016-815, 2016
Manuscript under review for journal Atmos. Chem. Phys.
Published: 15 September 2016

Atmospheric Chemistry and Physics Discussions

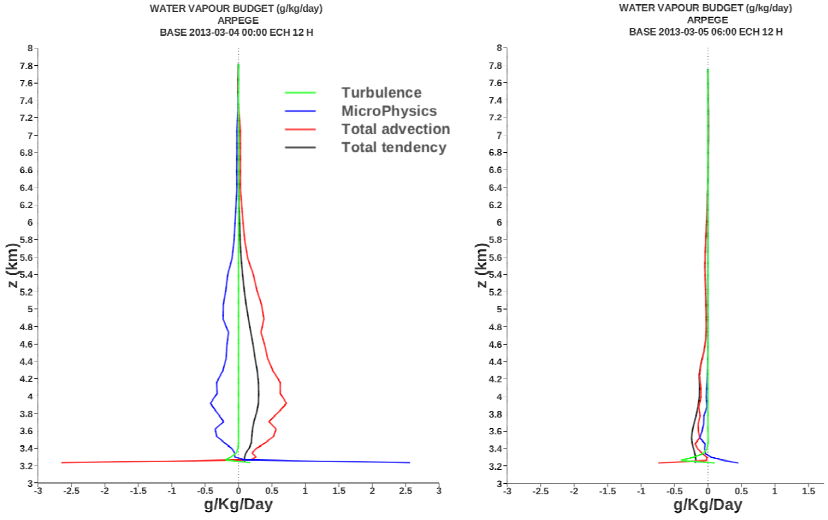

964

965 **Fig. 18:** (Left) Water vapour budget calculated by ARPEGE on 4 March 2013 over the 12-h
966 period 00:00-12:00 UTC induced by turbulence (green), microphysics (blue), total advection
967 (red) showing the total tendency (black). (Right) Same as Left but on 5 March 2013 over the
968 12-h period 06:00-18:00 UTC.

969

970